# Inherited human ezrin deficiency impairs adaptive immunity

**Blanca García-Solís, PhD,[a,b,c] Ana Van Den Rym,[a,b,c] Laura Martinez-Martínez, MD,[d] Teresa Franco, MD,[d] Jareb J. Pérez-Caraballo, PhD,[e,f] Janet Markle, PhD,[e,f] Carolina Cubillos-Zapata, PhD,[b,g] Ana V. Marín, PhD,[h] María J. Recio, PhD,[c,h] José R. Regueiro, PhD,[h] Alfonso Navarro-Zapata, PhD,[i] Carmen Mestre-Durán, PhD,[i] Cristina Ferreras, PhD,[i] Carla Martín Cotázar, PhD,[i] Roció Mena, PhD,[j] Carlos de la Calle-Fabregat, PhD,[k] Alberto López-Lera, PhD,[l] Miguel Fernández Arquero, MD, PhD,[c,m] Antonio Pérez-Martínez, MD, PhD,[i] Eduardo López-Collazo, PhD,[b] Silvia Sánchez-Ramón, MD, PhD,[c,m] Jean-Laurent Casanova, MD, PhD,[n,o,p,q] Rubén Martínez-Barricarte, PhD,[e,f] Oscar de la Calle-Martín, MD, PhD,[d] and Rebeca Pérez de Diego, PhD[a,b,c]**

*Madrid and Barcelona, Spain; Nashville, Tenn; Paris, France; and New York, NY*

**Background: Inborn errors of immunity (IEI) are a group of monogenic diseases that confer susceptibility to infection, autoimmunity, and cancer. Despite the life-threatening consequences of some IEI, their genetic cause remains unknown in many patients.**

**Objective: We investigated a patient with an IEI of unknown genetic etiology.**

**Methods: Whole-exome sequencing identified a homozygous missense mutation of the gene encoding ezrin *(EZR)*, substituting a threonine for an alanine at position 129.**

**Results: Ezrin is one of the subunits of the ezrin, radixin, and moesin (ERM) complex. The ERM complex links the plasma membrane to the cytoskeleton and is crucial for the assembly of an efficient immune response. The A129T mutation abolishes basal phosphorylation and decreases calcium signaling, leading to complete loss of function. Consistent with the pleiotropic function of ezrin in myriad immune cells, multidimensional immunophenotyping by mass and flow cytometry revealed that in addition to hypogammaglobulinemia, the patient had low frequencies of switched memory B cells, $CD4^+$ and $CD8^+$ T cells, MAIT, γδ T cells, and $^{central}$naive $CD4^+$ cells.**

**Conclusions: Autosomal-recessive human ezrin deficiency is a newly recognized genetic cause of B-cell deficiency affecting cellular and humoral immunity. (J Allergy Clin Immunol 2023;■■■:■■■-■■■.)**

***Key words:*** *Primary immunodeficiency, inborn errors of immunity, antibody deficiency,* EZR*, lymphoid cells, mass cytometry, computational immunology, next-generation sequencing*

Inborn errors of immunity (IEI) are a heterogeneous group of monogenic diseases conferring susceptibility to infection, autoimmunity, and cancer. Genetic analysis of patients with IEI has paved the way for the genetic diagnosis of patients, counseling for families, and preventive treatments for individuals at risk. These studies have greatly improved diagnosis and outcome for many affected patients. Furthermore, in terms of basic science, IEI have been instrumental in shedding light on the mechanisms of human immunity.[1] Nevertheless, no genetic diagnosis has yet been obtained for a large proportion of patients with IEI, highlighting the continuing need for studies in these patients.

The ezrin, radixin, and moesin (ERM) proteins are a family of proteins that act as linkers between the plasma membrane and the cytoskeleton, playing a role in endothelial cells and both the innate and adaptive arms of immunity. ERMs are characterized by the presence of a ~300 amino acid plasma membrane–associated FERM (4.1 protein, ezrin, radixin, and moesin) domain, followed by a long region with a high α-helical propensity and terminating in a C-terminal domain (also known as C-ERMAD, for C-terminal ERM-association domain) that has the ability to bind the FERM domain or F-actin.[2] They regulate the association of cortical actin with membrane-associated proteins in cell substructures by binding directly to both.[3,4] These proteins are highly versatile, with roles in the regulation of cell motility, protein localization, cellular architecture, and signaling. Phosphorylation of a conserved C-terminal threonine residue is critical for their conformational activation and membrane–actin cross-linking

From [a]the Laboratory of Immunogenetics of Human Diseases, IdiPAZ Institute for Health Research, La Paz University Hospital, Madrid; [b]the Innate Immunity Group, IdiPAZ Institute for Health Research, La Paz University Hospital, Madrid; [c]the Interdepartmental Group of Immunodeficiencies, Madrid; [d]the Immunology Department, Hospital de la Santa Creu i Sant Pau, Barcelona; [e]the Division of Genetic Medicine, Department of Medicine, Vanderbilt Genetics Institute, Vanderbilt University Medical Center, Nashville; [f]the Division of Molecular Pathogenesis, Department of Pathology, Microbiology, and Immunology, Vanderbilt Center for Immunobiology, Vanderbilt Institute for Infection, Immunology, and Inflammation, Vanderbilt University Medical Center, Nashville; [g]the Centre for Biomedical Research Network, CIBEres, Madrid; [h]the Department of Immunology, Ophthalmology and ENT, Complutense University School of Medicine, and 12 de Octubre Health Research Institute (imas12), Madrid; [i]Translational Research in Paediatric Oncology, Haematopoietic Transplantation and Cell Therapy, IdiPAZ Institute for Health Research, La Paz University Hospital, Madrid; [j]the Institute of Medical and Molecular Genetics (INGEMM), Hospital Universitario La Paz, Universidad Autónoma de Madrid, IdiPAZ, Madrid; [k]the Epigenetics and Immune Disease Group, Joseph Carreras Research Institute (IJC), Badalona, Barcelona; [l]the IdiPAZ Institute for Health Research, La Paz University Hospital, CIBERER U-754, Madrid; [m]the Clinical Immunology Department, San Carlos Clinical Hospital, Madrid; [n]the Laboratory of Human Genetics of Infectious Diseases, Necker Branch, Institut National de la Santé et de la Recherche Médicale U1163, Paris; [o]the St Giles Laboratory of Human Genetics of Infectious Diseases, Rockefeller Branch, The Rockefeller University, New York; [p]the Imagine Institute, University Paris Descartes, Paris; and [q]the Howard Hughes Medical Institute, New York.

The first 2 authors contributed equally to this article, and both should be considered first author.

Received for publication January 13, 2023; revised May 31, 2023; accepted for publication May 31, 2023.

Corresponding author: Rebeca Pérez de Diego, PhD, Laboratory of Immunogenetics of Human Diseases, IdiPAZ Institute for Health Research, La Paz University Hospital, P° Castellana, 261 Madrid, Madrid 28046, Spain. E-mail: rebeca.perez@idipaz.es.

0091-6749



https://doi.org/10.1016/j.jaci.2023.05.022

*Abbreviations used*
APC: Allophycocyanin
CADD: Combined annotation-dependent depletion
CFSE: Carboxyfluorescein succinimidyl ester
EBV-B: Epstein-Barr virus–transformed B
ERM: Ezrin, radixin, and moesin
*EZR*: Ezrin
FBS: Fetal bovine serum
FERM: 4.1 protein, ezrin, radixin, and moesin
FITC: Fluorescein isothiocyanate
IEI: Inborn errors of immunity
MAIT: Mucosal-associated invariant T
MEM: Marker enrichment modeling
NK: Natural killer
PBMC: Peripheral blood mononuclear cell
PHA: Phytohemagglutinin
WT: Wild type

function.[2] The only known IEI affecting the ERM complex identified to date result from mutations affecting moesin function.[5-7] Nine patients with moesin deficiency have been described, all with profound lymphopenia, hypogammaglobulinemia, fluctuating monocytopenia, and neutropenia. Two mutations have been identified in these patients: a missense R171W mutation in 8 patients and a nonsense R553X mutation in the ninth patient.[5-7] These patients have poor immune responses to vaccine antigens and are particularly susceptible to bacterial and varicella zoster virus infections. Most of their $CD8^+$ T cells express the senescence marker CD57, a phenotype associated with the impaired T-cell proliferation observed in these patients.[5-7] A similar lymphopenia phenotype has been observed in moesin-deficient mice, which develop a systemic lupus erythematosus–like autoimmune phenotype.[8] In both humans and mice, moesin deficiency mostly affects naive T cells, resulting in particularly small numbers of naive $CD8^+$ T cells.

Studies in radixin-deficient mice have indicated a role for this protein in the liver, where it is required for the secretion of conjugated bilirubin, with the support of Mrp2.[9,10] Radixin deficiency also affects hearing by impairing the maintenance of developed cochlear stereocilia.[11] Ezrin has been shown to compensate for radixin deficiency, highlighting the complicated functional redundancy of ERM proteins *in situ.* No defects of either the radixin or ezrin proteins have ever been reported in humans. We therefore searched our database for patients with the corresponding defects.

## METHODS

### Study approval

The experimental protocol was approved by the ethics committee of La Paz University Hospital (Madrid, Spain), and written informed consent was obtained from the patient's family for participation in this study.

### Human molecular genetics and whole-exome sequencing

Genomic DNA was extracted from whole blood with a kit (Qiagen, Venlo, The Netherlands) in accordance with the manufacturer's instructions. Whole-exome sequencing was performed on genomic DNA from whole blood by the New York Genome Center with an Illumina HiSeq 2500 machine (Illumina, San Diego, Calif) and an Agilent 71Mb SureSelect exome kit (Agilent Technologies, Santa Clara, Calif). The reads were aligned with the human reference genome and with a BWA aligner,[12] then recalibrated and annotated with GATK,[13] PICARD (picard.sourceforge.net), and ANNOVAR.[14] The variants were then filtered and investigated by using our in-house online server.

The whole-exome sequencing results were validated by PCR and sequencing analysis on genomic DNA from whole blood. PCR was performed with PCR Master Mix (Promega, Madison, Wis) and the GeneAmp 9700 PCR System (Applied Biosystems; Thermo Fisher Scientific, Waltham, Mass). The primer sequences used for the ezrin coding region were as follows: EZR-1 forward: gggcgctctaagggttct; EZR-1 reverse: atcgtcttctgcgtgtgaga; EZR-2 forward: ccacactgag gagcagctta; EZR-2 reverse: gcttcgcaaacaaaataactga; EZR-3 forward: tggggactctgctagaccat; EZR-3 reverse: acagggtgagttgctccagt; EZR-4 forward: gccccattgagtcttggtta; EZR-4 reverse: gcatgaaggag cacttgaca; EZR-5 forward: gatttgaatggaaagtaagggttt; EZR-5 reverse: tcacaaggcctgacacagag; EZR-6 forward: cattgagcccatccta caca; EZR-6 reverse: taacccacaaatttgccatt; EZR-7 forward: attgtgcctcttgggttagc; EZR-7 reverse: ctggccctcaatgtaacctc; EZR-8 forward: tctggacctttgtgaaggatg; EZR-8 reverse: ggttccattccacca cactc; EZR-9 forward: ccctcaggataccaagtcca; EZR-9 reverse: tcatttcggctgtgagtctg; EZR-10 forward: ccctcaacctgtgacttggt; EZR-10 reverse: cccccagcagatcagtttac; EZR-11 forward: gcttgccaacaca catgaac; EZR-11 reverse: cagcttgagccagacctctc; EZR-12 forward: agttcagtgctgccttagcc; EZR-12 reverse: cccctaggaaaacaggaagg; EZR-13 forward: ttgcccttcctgttttccta; EZR-13 reverse: gccca gaatgtttctgttgg. PCR products were purified with the QIAquick Gel Extraction Kit (Qiagen) and sequenced with the BigDye Terminator Cycle Sequencing Kit (Applied Biosystems). Sequencing products were purified by precipitation in 70% ethanol, and their sequences were analyzed with an ABI Prism 3700 genetic analyzer (Applied Biosystems).

### Alignment of multiple amino acid sequences

The *Homo sapiens* ezrin (NP_003370.2) amino acid sequence was aligned with other ezrin sequences with the Basic Local Alignment Search Tool and the protein database of the US National Center for Biotechnology Information (blast.ncbi.nlm.nih.gov/Blast.cgi). Multiple sequence alignment was performed with AlignmentViewer, a program for multiple sequence alignment (alignmentviewer.org), with the ezrin amino acid sequences of *Mus musculus* (NP_033536.2), *Struthio camelus* (KFV87607.1), *Chelonoidis abingdonii* (XP_032649155.1), *Callorhinchus milii* (AFO94923.1), *Danio rerio* (NP_0010183 26.1), *Latimeria chalumnae* (XP_014352395.1), and *Petromyzon marinus* (ENSPMAP00000008006).

### Protein structure modeling

The active FERM domain of human ezrin (1NI2) was represented in Swiss-PdbViewer with the A129T mutation.

### Cell purification and culture

Human peripheral blood mononuclear cells (PBMCs) were isolated by Ficoll-Hypaque density gradient centrifugation (Amersham Pharmacia Biotech, Piscataway, NJ) of whole-blood samples

obtained from the patient, her relatives, or healthy volunteers. As previously described, Epstein-Barr virus–transformed B (EBV-B) cell lines were obtained from the patient and healthy donors.[15] EBV-B cells were cultured in RPMI 1640 medium (GlutaMAX, Thermo Fisher Scientific) supplemented with 10% fetal bovine serum (FBS) (Thermo Fisher Scientific).

Jurkat T cells (American Type Culture Collection [ATCC], Manassas, Va) were cultured in RPMI 1640 medium (GlutaMAX, Thermo Fisher Scientific) supplemented with 10% FBS (Thermo Fisher Scientific).

## Immunoblot analysis

Total cell extracts were prepared from PBMCs and EBV-B cells, either untransfected or transfected by nucleofection with pcDNA3.1-ezrin or pcDNA3.1 (mock). Equal amounts of protein from each sample were separated by sodium dodecyl sulfate–polyacrylamide gel electrophoresis and blotted onto iBlot Gel Transfer Stacks (Thermo Fisher Scientific). These nitrocellulose membranes were then probed with rabbit polyclonal antibodies directed against ezrin (PA5-86597, Thermo Fisher Scientific), mouse monoclonal antibodies directed against Tyr146-phosphorylated ezrin (sc-166858, Santa Cruz Biotechnology, Santa Cruz, Calif), or rabbit polyclonal antibodies directed against Tyr353-phosphorylated ezrin (3144, Cell Signaling Technology, Danvers, Mass), followed by a horseradish peroxidase–conjugated anti-rabbit IgG secondary antibody (Cell Signaling Technology). Membranes were stripped and reprobed with an antibody against glyceraldehyde-3-phosphate dehydrogenase (aka GADPH) (Abcam, Cambridge, United Kingdom) to control for protein loading. Antibody binding was detected by enhanced chemiluminescence (NZYTech, Lisbon, Portugal).

## Mass cytometry

**Staining and data acquisition.** In total, $5 \times 10^6$ PBMCs were stained with Cell-ID Cisplatin-$^{195}$Pt (Fluidigm [now Standard BioTools], South San Francisco, Calif) to detect dead cells. The PBMCs were then subjected to FcR blockade with Human TruStain FcX blocking solution (BioLegend, San Diego, Calif), stained with the antibody mixture, as previously described[16] (see Table E1 in this article's Online Repository at www.jacionline.org), fixed with 1.6% paraformaldehyde, and stained with Cell-ID intercalator-Ir. The stained PBMCs were then analyzed in a Helios CyTOF 3.0 cytometer (Fluidigm) at the Vanderbilt University Cancer and Immunology Core. The data were exported as a flow cytometry standard (FCS) file and normalized against EQ bead standards (Fluidigm) according to the manufacturer's protocol.

**Data analysis.** For the multidimensional analysis, the data were pregated to remove dead cells and debris, and leukocytes were selected by FlowJo v10.7.2 (Becton Dickinson, Franklin Lakes, NJ), as previously described.[16] The pregated data were exported as an FCS file and imported into RStudio (rstudio.com). We used the CATALYST package[17] for the arcsine transformation of marker intensities with a cofactor of 5 and subsequent analysis. FlowSOM was used for unsupervised clustering,[18] the R package 'ggplot2' was used for data representation, and MEM[19] was used for the characterization of the different clusters. Manual gating was performed in FlowJo, as previously described.[16] Population frequencies were exported from FlowJo and analyzed by Prism 9 (GraphPad Software, La Jolla, Calif).

## Flow cytometry study of lymphocyte subpopulations

T-cell and B-cell subpopulations were evaluated with whole-blood samples collected into EDTA, cell-surface marker staining, and standard flow cytometry methods. The T-cell subpopulation samples were incubated with antibodies directed against CD3 fluorescein isothiocyanate (FITC) or BV510 or PerCP-Cy5.5, CD4 BUV395 or allophycocyanin (APC) or V500-C, CD8 PerCP (Miltenyi Biotec, San Diego, Calif) or PerCP-Cy5.5 or APC, CD45RA BV650 or FITC, CD45RO BV510 or APC-VIO700, CXCR3 BV421, CCR6 BV605, CD25 BV786, CD127 PE, CCR7 BV605, CD31 PE-Cy7, and TCR γδ FITC (BD Biosciences, Franklin Lakes, NJ) for 20 minutes. B-cell samples were stained with a mixture of the antibodies against the following proteins, at optimal concentrations: CD27 FITC or APC, CD19 PerCP 5.5 or BV510, CD21 FITC, CD38 PE-Cy7, CD24 PerCP-Cy5.5, and anti-IgD PE (BD Biosciences). Natural killer (NK) cell samples were stained with a mixture of antibodies against the following proteins, at optimal concentrations: CD3 FITC and CD56 PerCP 5.5. The cells were washed and resuspended in 0.2 mL 1× PBS for acquisition in a BD FACSCelest cell analyzer. Data were analyzed by FlowJo v10.8.

Events were then gated on a lymphocyte gate based on forward-scatter (FSC-A) versus side-scatter area (SSC-A). Initial gating involved the use of a forward-scatter width (FSC-W) versus height (FSC-H) plot and side-scatter width (SSC-W) versus height (SSC-H) plot to remove doublets. Events were further gated on CD3, CD4, and CD8 for T cells and on CD19 for B cells. After their identification, T cells were analyzed and classified on the basis of their expression of CD45RO, CD45RA, CD25, CD127, CXCR3, and CCR6 into regulatory T, $T_H1$, $T_H2$, and $T_H17$ cells, and on the basis of their expression of CD45RO, CD45RA, and CD31 for $^{thymic}$naive and $^{central}$naive CD4$^+$ T cells. B cells were then analyzed and classified on the basis of their expression of IgM, IgD, and CD27 into naive or switch memory B cells, and NK cells were identified as CD3$^-$CD56$^+$ cells.

## Carboxyfluorescein succinimidyl ester proliferation assay for T cells

Peripheral blood mononuclear cells (PBMCs) ($10 \times 10^6$ cells/mL) were incubated at 37°C for 10 minutes with carboxyfluorescein succinimidyl ester (CFSE) at a concentration of 2 μmol and were then washed twice with cold 10% FBS in RPMI 1640. The cells were cultured for 6 days at a density of $10^6$ cells/mL in 10% FBS in RPMI 1640 in 24-well tissue culture plates at 37°C under an atmosphere containing 5% $CO_2$. The cells were left unstimulated or were stimulated with phytohemagglutinin M Gibco; Thermo Fisher Scientific) at a concentration of 0.4% vol/vol, or with human T-activator CD3/CD28 beads (Dynal, Invitrogen; Thermo Fisher Scientific, Waltham, Mass) at a bead-to-cell ratio of 1:1 according to the manufacturer's instructions. The cells were collected after 6 days and labeled with CD3 BV510 VioGreen (BD Biosciences), CD4 BV395 (BD Biosciences), and CD8 PercP (Miltenyi Biotec) or without fluorochromes for the measurement of cell autofluorescence. After 20 minutes' incubation, the cells were washed with PBS and resuspended in 0.2 mL

PBS for acquisition in a BD FACSCelesta cell analyzer. A magnet was used to remove the beads before acquisition for cells stimulated with human T-activator CD3/CD28 beads. On day 0, the CFSE signal was measured by flow cytometry, to adjust the settings. Data were analyzed by FlowJo.

### *In vitro* migration

*In vitro* Transwell migration assays were performed in Boyden chambers with 6.5 mm Transwell filters with 3.0 μm pore polycarbonate membrane inserts (Corning, Corning, NY) coated with fibronectin (20 μg/mL, lyophilized human plasma FN; Sigma-Aldrich, St Louis, Mo). We resuspended $5 \times 10^5$ EBV-B or PBMC cells in 0.1 mL RPMI 1640 and placed them in the upper chamber of the precoated Transwells, in triplicate. The lower chamber was filled with RPMI 1640 and RPMI 1640 supplemented with 10% FBS as a chemoattractant. Transwells were incubated for 24 h at 37°C in a humidified incubator in the presence of 5% $CO_2$. The cells that had migrated were then recovered from the lower chamber of the Transwell and quantified by flow cytometry with 100 μL of cells and 100 μL of counting beads (Flow-Count Fluorospheres; Beckman Coulter, Fullerton, Calif) in a Navios cytometer. PBMC recovered from the lower chamber were previously incubated with CD3 PE and CD19 FITC (BD Biosciences).

### Calcium flux

EBV-B cells from the patient and healthy donors were loaded with Fluo-4 (Molecular Probes; Thermo Fisher Scientific) by electroporation. Some of the patient's cells were left untransfected or were transfected with pcDNA3.1-*ezrin* or pcDNA3.1 (mock) and then stimulated with 2.5 ng/μL ionomycin (Sigma-Aldrich). Fluorescence was measured in a BD FACSCelesta flow cytometer, and the data were analyzed by FlowJo (Kinetics). The histograms show the populations gated on the basis of forward scatter versus side scatter and singlets. The data shown are representative of 3 different experiments.

### Mutagenesis and transient transfections

Full-length wild-type (WT) ezrin cDNA was generated by NZYTech using pCDNA3.1 as the vector. EBV-B cells were transfected with a nucleofection device (Lonza, Basel, Switzerland) and the Amaxa Cell Line Nucleofector Kit V (Lonza) according to the manufacturer's instructions. The A-024 program was used for EBV-B cell transfection ($5 \times 10^6$ cells per 5 μg of plasmid).

For Jurkat T-cell studies, various ezrin variants were generated from the full-length WT ezrin in plasmids, with a mutagenesis kit (NZYTech) used according to the manufacturer's instructions and with the following primers: A129T forward: GTGCTC TTGGGGTCCTACACTGTGCAGGCCAAGTTTG; A129T reverse: CAAACTTGGCCTGCACAGTGTAGGACCCCAAGAGCAC; G109X forward: CTTCCTCCAAGTGAAGGAATGAATCCTTAGCGATGAG; G109X reverse: CTCATCGCTAA GGATTCATTCCTTCACTTGGAGGAAG.

Mutagenesis was confirmed by Sanger sequencing.

Jurkat T cells were transfected with a nucleofection device (Lonza) and the Amaxa Cell Line Nucleofector Kit V (Lonza) according to the manufacturer's instructions. The U-029 program was used for the transfection of Jurkat T cells ($1.8 \times 10^6$ cells per 2 μg of plasmid).

### Cytokine determinations

Cytokine production was assessed in nonstimulated EBV-B cells and Jurkat T cells left unstimulated or stimulated with phytohemagglutinin M (Gibco) at a concentration of 0.4% vol/vol. Cell supernatants were recovered in accordance with the manufacturer's instructions, and the concentration of IL-10 or IL-2 was determined by ELISA (BioLegend).

### Statistical analysis

Data were collected from a minimum of 3 experiments and are expressed as means ± SDs. As a result of the small sample size, statistical significance was assessed by Kruskal-Wallis (nonparametric) tests comparing the differences between healthy donors and the patient in the same conditions. Differences between samples were considered statistically significant if $P < .05$. Statistical analysis was performed by GraphPad Prism v8.4.0.

## RESULTS

### Homozygous *EZR* mutation was found in a patient with B-cell deficiency

We studied a 30-year-old European woman from Spain (P1). This patient, who was born to consanguineous parents (Fig 1, *A*), had suspected B-cell deficiency of unknown genetic origin, with progressive hypogammaglobulinemia (see Table E2 in the Online Repository at www.jacionline.org) and thrombocytopenia (see Table E3 in the Online Repository). The pregnancy and growth of P1 were normal, and P1 has 3 healthy siblings (2 sisters and 1 brother, all older than her) and 2 healthy nephews. Her mother had experienced pneumonia events. P1 had had vaginal candidiasis, pinworms at the age of 20 years, and eczema on the hands. She had also had infections due to *Giardia lamblia.* After vaccination, she had mounted weak serologic responses to hepatitis B and measles, negative serologic response to rubella, and weak serologic and cellular responses (QuantiFERON-COVID-19) to vaccine directed against severe acute respiratory syndrome coronavirus 2 spike (mRNA-1273). HLA class I expression was normal. High-resolution typing of HLA by next-generation sequencing revealed heterozygosity.

Whole-exome sequencing identified a biallelic missense variant in exon 4 of *EZR* on chromosome 6 that segregated with the disease in this kindred as an autosomal-recessive trait (Fig 1, *B*). This mutation replaces an alanine with a threonine at position 129 (g.158785391G>A [GRCh38.p12], c.385G>A, p.A129T) (Fig 1, *C*). This variant (rs528409234) is present in the Genome Aggregation Database (gnomAD; gnomad.broadinstitute.org) in the heterozygous state, with a minor allele frequency of 0.0001803, or 0.000268 in the non-Finnish European population, and exclusively in the heterozygous state and 0.00002 in the Trans-omics for Precision Medicine (TOPMed; imputation.biodatacatalyst.nhlbi.nih.gov) database, consistent with the prevalence of B-cell deficiency in the general population. The variant was validated by Sanger sequencing of genomic DNA from peripheral leukocytes, which confirmed that the patient's mother and 2 sisters were heterozygous for this mutation (Fig 1, *A* and *B*). It was not possible to test the father. No other

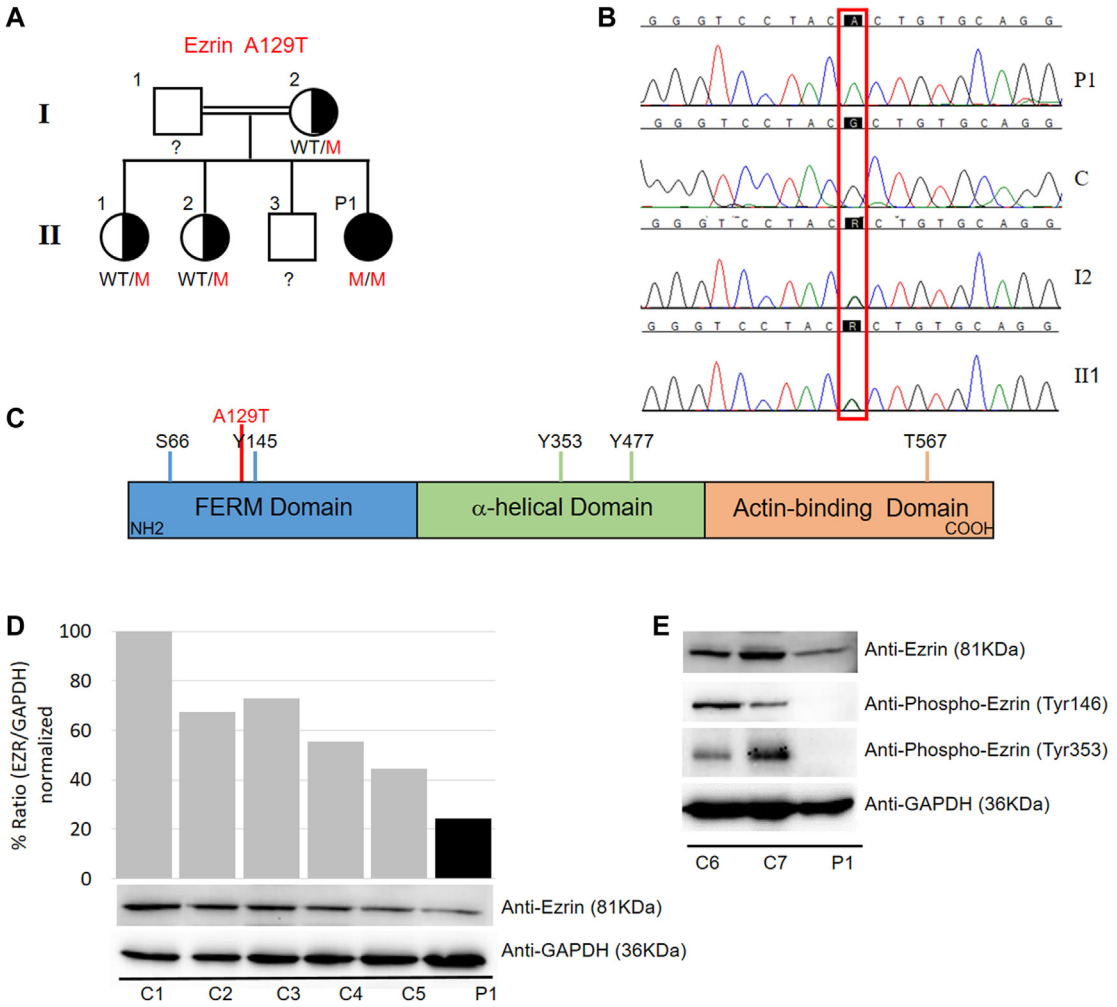


**FIG 1.** Biallelic ezrin variant in patient with B-cell deficiency. **(A)** Familial segregation of ezrin A129T mutation. **(B)** Sanger sequencing results for region encompassing mutation for patient (P1), healthy control (C), patient's mother (I2), and patient's sister (II1). **(C)** Representation of ezrin protein indicating various domains and position of main phosphorylation sites and A129T mutation. **(D)** Immunoblot analysis of ezrin protein in PBMCs from P1 and 5 healthy age-matched controls (C1–C5). GAPDH was used as loading control. Ezrin quantification was normalized against intensity of band for GAPDH. Results are shown from a single experiment, representative of 3. **(E)** Immunoblot analysis of ezrin proteins phosphorylated on tyrosine 146 and 353 residues in PBMCs from P1, C6, and C7. GAPDH was used as loading control. Results are shown from a single experiment, representative of 3. *GAPDH,* Glyceraldehyde phosphate dehydrogenase.

mutations were found in the *EZR* coding region. Ezrin is composed of 586 amino acids forming 3 principal domains: an N-terminal FERM (4.1 ezrin, radixin, moesin) domain that binds to transmembrane and adaptor proteins, an α-helical domain, and a C-terminal domain that binds to filamentous actin (Fig 1, *C*).[20] By aligning the ezrin protein sequences of humans and other species, we were able to show that A129 was highly conserved throughout the evolution of vertebrates, including agnathans (Fig 2, *A*). The replacement of an alanine residue with a threonine residue is predicted to modify the polarity of the region as a result of the replacement of a nonpolar amino acid with a polar amino acid, and to generate steric hindrance as a result of the larger size of the threonine residue (Fig 2, *B*). The combined annotation-dependent depletion (CADD) score for this variant is way above the mutation significance cutoff, suggesting that this mutation may be deleterious (Fig 2, *C*).[21] Furthermore, according to the *f* parameter, *EZR* is under strong purifying selection, indicating that mutations of this gene would be likely to have severe functional consequences (Fig 2, *D*).[22] In total, 17 *EZR* variants in the homozygous state have been reported in public databases, all with a CADD score below that of the A129T variant (Fig 2, *E* and *F*). These results suggest that this biallelic germline missense *EZR* mutation (g.158785391G>A; p.A129T, rs528409234) may underlie a newly discovered autosomal-recessive form of combined immunodeficiency disease.

## Ezrin A129T mutation results in loss of function

We assessed the functional consequences of the A129T variant for ezrin function. We first investigated the effect of the mutation on the production of ezrin protein. By immunoblotting PBMCs from the patient and age-matched healthy controls, we showed that ezrin protein levels were slightly lower in the patient (Fig 1, *D,*

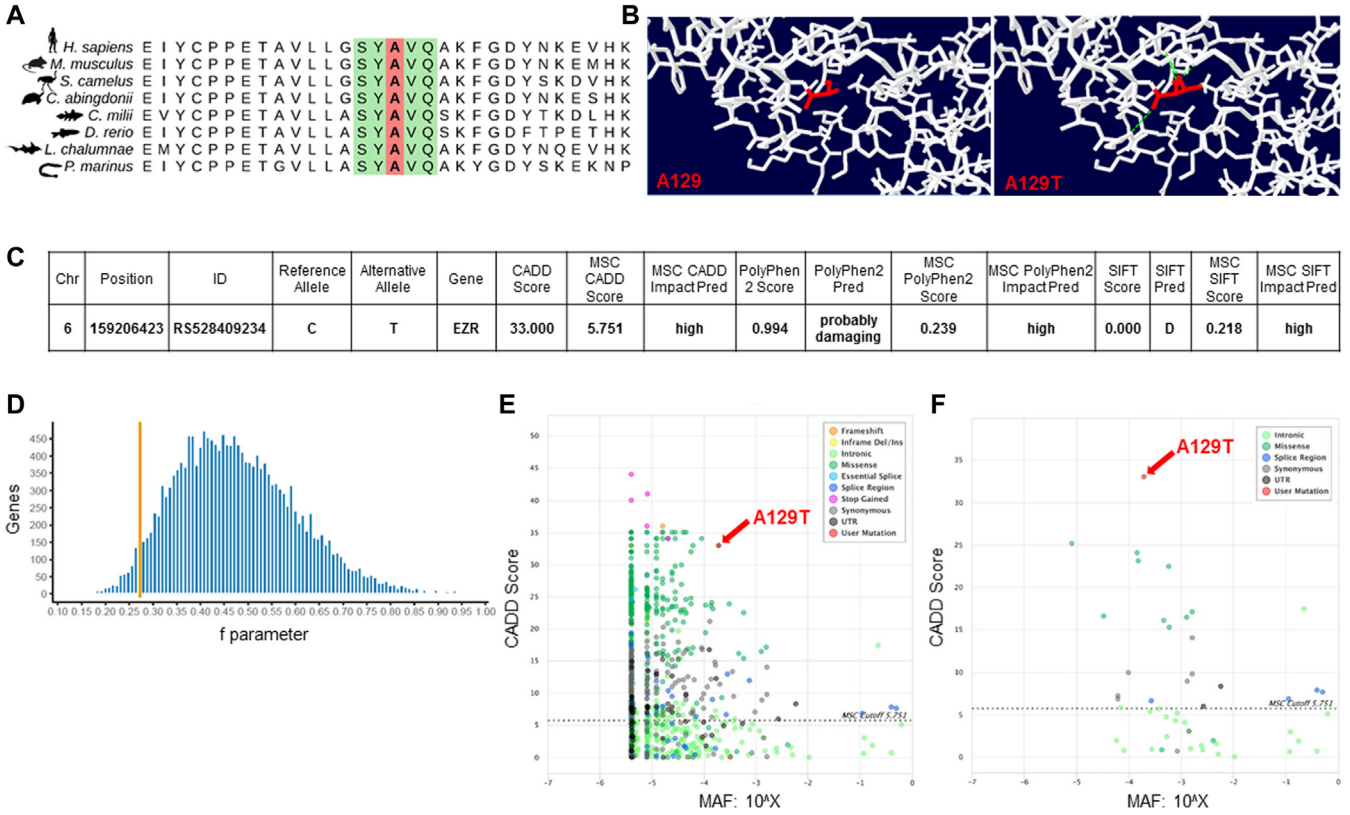


**FIG 2.** *In silico* studies of *EZR* mutation. **(A)** Multiple alignments of human ezrin sequence with ezrin sequences from 7 other species, showing conservation of A129 residue in all 8 species analyzed. **(B)** *Left,* A129 *(red)* within FERM domain of human ezrin.[20] *Right,* A129T mutation. Created with Swiss-PdbViewer. **(C)** MSC (pec630.rockefeller.edu:8080/MSC) for ezrin A129T mutation. **(D)** Gene Damage Index (lab.rockefeller.edu/casanova/GDI) for *EZR.* **(E)** Population genetics visualization generated by PopViz (shiva.rockefeller.edu/PopViz) (CADD score versus minor allele frequency [MAF]) for all variants of human ezrin, with A129T indicated in *red.* **(F)** Population genetics visualization generated by PopViz of homozygous variants of human ezrin, with A129T indicated in *red. MSC,* Mutation significance cutoff.

and see Table E4 in the Online Repository at www.jacionline.org). Phosphorylation is a critical step in the activation of ezrin. Ezrin may exist as a monomer, dimer, or oligomer, depending on its activation state. In the monomeric form, the N-terminal domain of the protein associates with the C-terminal actin-binding domain in an intramolecular interaction, masking the binding site (inactive state). Parallel or antiparallel dimers or head-to-tail oligomers, generated by the phosphorylation of different amino acid residues located in the N and C termini, constitute the active forms.[3] In the absence of activation, receptors, such as B-cell receptor, are trapped within surface compartments created by the anchoring of the plasma membrane to the actin cytoskeleton by ezrin, leading to the phosphorylation and activation of the ezrin protein, restricting its diffusion. We therefore decided to investigate ezrin phosphorylation at positions 146 (Tyr 146) and 353 (Tyr353), which are important for signal transduction.[3,23] We detected basal ezrin phosphorylation in the PBMCs of 2 healthy age-matched donors, with a complete absence of Tyr146 and Tyr353 phosphorylation in P1's PBMCs (Fig 1, *E*). Thus, the patient's *EZR* mutation decreases the amount of protein in the PBMCs and ezrin phosphorylation in basal conditions, with the phosphorylated conformation being the predominant state of the protein in healthy circulating lymphocytes, in which it maintains cell rigidity. The patient therefore had autosomal-recessive ezrin deficiency.

## Ezrin deficiency is implicated in T-cell lymphopenia

Studies of ezrin-deficient mice have implicated ezrin in several adaptive immune cell functions.[24-26] Ezrin is strongly expressed by lymphoid precursor cells but is dispensable for T-cell development in mice.[24] Given the pleiotropic role of ezrin in leukocytes, we assessed the composition of patient's circulating immune system by in-depth immunophenotyping by mass cytometry. Visualization with the *t*-distributed stochastic neighbor embedding algorithm for dimensional reduction revealed marked differences in the distribution of leukocyte populations between a healthy control and the patient (Fig 3, *A-C*). Unsupervised clustering followed by manual clustering (Fig 3, *A-C,* Fig E1) showed $CD4^+$ and $CD8^+$ T-cell lymphopenia and low frequencies of mucosal-associated invariant T (MAIT) cells and γδ T cells (Fig 3, *D*). This reduction in the size of leukocyte subpopulations was further confirmed by manual gating (Fig E1). We investigated the effects on specific T-cell subpopulations by mass and classical cytometry to evaluate these subpopulations (Table I and Figs E2 and E3). The 2 analyses showed the proportions of the various subpopulations considered, including terminally differentiated effector memory (aka TEMRA), naive, central memory, effector memory, $T_H1$, $T_H1^*$, $T_H2$, and $T_H17$ cells, to be normal. However, an analysis of naive T cells showed that almost all these cells were $^{thymic}$naive $CD4^+$ T cells, and that the patient had lower levels

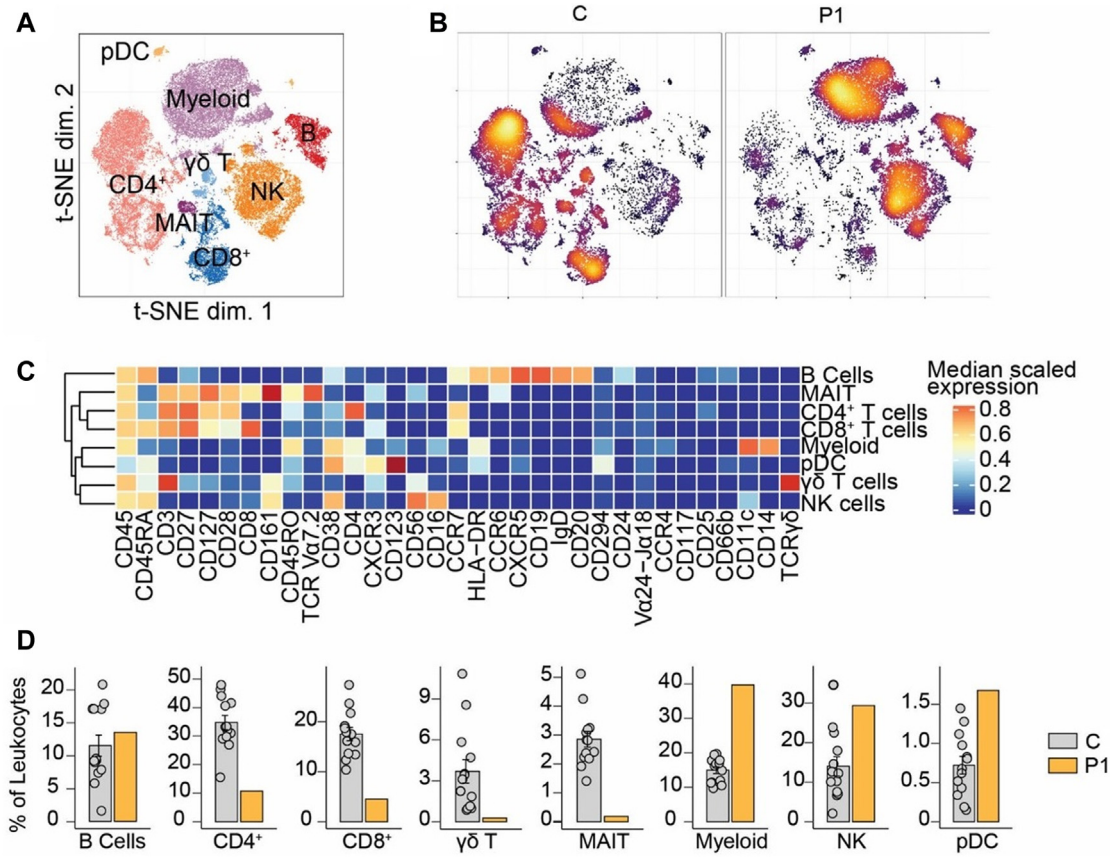


**FIG 3.** Leukocyte immunophenotyping. **(A)** Dimensional reduction by t-SNE of 33 markers used for immunophenotyping by mass cytometry. Each *color* represents cell population obtained by manual clustering by surface marker expression; 25,000 cells from healthy controls (C) and patient (P1) are represented. **(B)** t-SNE density showing leukocyte distribution for C and P1. **(C)** Median expression heat map for markers indicated for populations shown in *(A)*. **(D)** Frequencies of populations highlighted in *(A)* as percentage of total leukocytes. *t-SNE, t*-Distributed stochastic neighbor embedding.

of $^{central}$naive CD4$^+$ T cells than healthy donors (Table I, Fig E3). Postthymic selection in the periphery was therefore impaired in the patient, leading to T-cell lymphopenia. Our data suggest that contrary to findings for the mouse model, ezrin is crucial for postthymic T-cell development in humans.

## Impaired memory B-cell development occurs in the absence of functional ezrin

Murine ezrin deficiency resulted in higher rates of B-cell proliferation and differentiation into antibody-secreting cells *ex vivo* and stronger T-cell–independent and –dependent responses to antigens *in vivo* in mice, with no effect on B-cell development.[25] The frequency of B cells was normal in the patient (Fig 3, *D*), although a difference in B-cell subpopulations was observed between the patient and healthy controls, suggesting a possible defect of the differentiation of different B-cell subpopulations (Fig 3, *B*). Unsupervised clustering analysis on the B-cell data from Fig 3 identified 6 major populations (Fig 4, *A*). The frequency of clusters 1, 2, 4, and 6 in the patient was much lower than in healthy controls (Fig 4, *B*). We used marker enrichment modeling (MEM) to study these clusters.[19] MEM in a machine-learning approach can identify the markers distinguishing each subpopulation, providing an unbiased automatic characterization of the subpopulations present. This analysis showed that clusters 1, 2, 4, and 6 were characterized by the expression of markers typical of the memory compartment, whereas clusters 3 and 5 expressed markers typical of naive B cells (Fig 4, *C*).[27,28] Manual gating confirmed this observation and showed that the patient had low levels of double-negative and switched memory B cells, whereas the naive and unswitched compartments were of similar size to those in healthy controls (Fig 4, *D* and *E*). A classical flow cytometry study of different B-cell subpopulations confirmed that the patient had a deficit of switched memory B cells (Table II).[29] No decrease in the size of any of the T- or B-cell subpopulations was found in any of the heterozygous carriers, and unsupervised clustering revealed no other defect in the myeloid or NK compartments (Fig 3, *D,* Table II, and Fig E1). Manual gating demonstrated showed the frequencies of nonclassical, classical, and intermediate monocytes, myeloid cells, and plasmacytoid dendritic cells to be similar to those of healthy controls (Fig E1). These results suggest that human ezrin is redundant for the development of myeloid and NK lineages, but not for T and B cells.

**TABLE I.** Distribution of T-cell subpopulations in peripheral blood

| Cell | P1 (frequency of parental population) | % Healthy controls (range) |
|---|---|---|
| Lymphocytes | 19.2 | 35.2-56.2 |
| $CD3^+$ T | 57.7 | 56.2-73.3 |
| $CD4^+$ T | 74.4 | 47.4-78.5 |
| $CD45RO^+CD45RA^-$ (T memory) | 65.1 | 21.5-48.3 |
| $CD45RO^+CD45RA^+$ (T naive and effector) | 23.9 | 19.1-33.8 |
| $CD45RO^+CD25^-CD127^+$ ($T_H$) | 91.8 | 43.9-71.9 |
| $CXCR3^+CCR6^+$ ($T_H1$*$T_H17$) | 20.7 | 3.93-12.0 |
| $CXCR3^+CCR6^-$ ($T_H1$) | 40.9 | 12.0-26.0 |
| $CXCR3^-CCR6^+$ ($T_H17$-$T_H22$) | 8.0 | 10.4-15.5 |
| CXCR3-CCR6- ($T_H2$) | 22.4 | 44.5-60.8 |
| $CD45RO^+CD25^+CD127^{low}$ (memory Treg) | 0.76 | 1.81-4.21 |
| $CXCR3^+CCR6^+$ ($T_H1$*$T_H17$-like Treg) | 17.9 | 2.32-16.4 |
| $CXCR3^+CCR6^-$ ($T_H1$-like Treg) | 46.2 | 4.2-25.8 |
| $CXCR3^-CCR6^+$ ($T_H17$-$T_H22$–like Treg) | 3.2 | 10.4-18.5 |
| $CXCR3^-CCR6^-$ ($T_H2$-like Treg) | 15.4 | 30.7-67.4 |
| $CD45RO^-CD45RA^+$ | 28.5 | 40.3-53.0 |
| $CD31^+$ ($^{thymic}$naive CD4 T) | 96.3 | 64.4-75.5 |
| $CD31^-$ ($^{central}$naive CD4 T) | 3.7 | 24.5-35.6 |
| $CD8^+$ T | 19.3 | 16.2-45.3 |
| $CD45RO^+$ $CD45RA^-$ (T memory) | 10.2 | 2.7-9.3 |
| $CD45RO^+CD45RA^+$ (T naive and effector) | 27.4 | 15.8-63.8 |
| $CCR7^+CD45RA^+$ (T naive) | 53.4 | 7.4-65.8 |
| $CCR7^+CD45RA^-$ (T central memory) | 17.3 | 3.6-23.0 |
| $CCR7^-CD45RA^-$ (T effector memory) | 25.2 | 7.0-39.1 |
| $CCR7^-CD45RA^+$ (T effector memory reexpressing *CD45RA*, TEMRA) | 4.2 | 4.5-17.1 |
| γδ T | 1.2 | 1.0-7.0 |

For the patient, values are presented as percentage of parental population. For healthy controls (adults), percentages of parental population are shown for internal reference. *TEMRA,* Terminally differentiated effector memory.

## Ezrin deficiency affects calcium flux in B cells

Given the predominantly B-cell defect of this patient, characterized by hypogammaglobulinemia and low levels of switched memory B cells, we further investigated the function of ezrin in human B-cell biology. Ezrin is involved in B-cell receptor,[4,25,30,31] Toll-like receptor 4 signaling,[32] and in B-cell migration.[33,34] An increase in intracellular calcium ion ($Ca^{2+}$) levels is one of the key signals triggering a B-cell response to antigens.[35] We therefore analyzed the impact of ezrin deficiency on calcium flux. We stimulated EBV-B cells with the calcium ionophore ionomycin and used Fluo4 dye to measure calcium mobilization. $Ca^{2+}$ mobilization levels were lower in patient cells than in control cells. This decrease in calcium flux was ezrin dependent because introduction of a WT ezrin allele into EBV-B cells from the patient restored normal response (Fig 5, *A-C*). Our data suggest that the A129T mutation affects $Ca^{2+}$ signaling, with potential consequences for immune response and clinical presentation of the patient.

## Ezrin deficiency alters IL-10 secretion but not chemotaxis in B cells

Studies in mice have shown that dephosphorylated ezrin induces an increase in the levels of anti-inflammatory IL-10.[32] Furthermore, the conditional deletion of ezrin in mouse B cells increases the amount of IL-10 production induced by Toll-like receptor 4 ligation.[32] Consistent with these findings for mice, EBV-B cells from the patient secreted large amounts of IL-10 in the basal state (Fig 5, *D*). These high basal levels of IL-10 in EBV-B cells were not associated with any clinical feature of the patient, but the relevant role of IL-10 as potent anti-inflammatory cytokine with both pro- and antitumor effects should be remembered.[36]

Conversely, ezrin has been reported to be involved in B-cell chemotaxis and migration.[33,34,37] We therefore investigated the effect of ezrin deficiency on B-cell chemotaxis. We used the Transwell system to assess cell migration toward the chemoattractant FBS (Fig 5, *E* and *F*). EBV-B cells from the patient migrated toward the membrane in a similar manner to the EBV-B cells of the controls. We found no significant difference in EBV-B cell migration between the patient and 5 healthy donors (Fig 5, *E* and *F*). The same results were obtained in primary cells (B and T cells) with no significant difference migration between the patient and healthy donors (Fig E4). Ezrin deficiency in the patient's B cells had no major effect on B-cell migration, consistent with her mild clinical phenotype. Despite having hypogammaglobulinemia and mild lymphopenia, the patient experienced none of the severe defects presented by patients with inherited disorders due to impaired leukocyte migration characterized by leukocyte trafficking defects (some of which are classified as severe combined immunodeficiencies).[38,39] This suggests that moesin can compensate for ezrin deficiency.

## T-cell signaling remains intact in ezrin deficiency

Given the clinical presentation of combined immunodeficiency disease with $CD4^+$ and $CD8^+$ T-cell lymphopenia, we hypothesized that ezrin deficiency might affect T-cell activation. We tested this hypothesis by activating PBMCs and assessing T-cell proliferation on the basis of incorporation of CFSE. Consistent with observations in mice,[26] we found no difference in proliferation between the patient and healthy controls after stimulation with phytohemagglutinin (PHA) and anti-CD3/CD28 antibody (CD3-CD28) (Fig E5). It is again consistent with the patient's mild clinical phenotype that despite her general T-cell lymphopenia, her T-cell proliferation was normal, attenuating the phenotype and suggesting that the defect is not intrinsic to circulating T cells.

## Altered IL-2 production is driven by ezrin A129T mutation

The analyses of T-cell proliferation described above used polyclonal stimuli potentially unable to identify more subtle differences. We therefore designed a system for studying TCR-dependent differences in a genotype-dependent manner in isolated cells. We used Jurkat T cells, which have been shown to be a suitable model for studying ezrin-dependent TCR activation.[40] We found that the membrane-binding domain of WT ezrin perturbed TCR clustering, inhibiting the activation of the nuclear factor for activated T cells.[40] We generated expression plasmids containing the A129T and G109X sequences as a negative control. We transfected Jurkat T cells with these plasmids, a plasmid containing the WT ezrin sequence, and an empty vector. We compared the functionality of the ezrin proteins encoded by these plasmids by assessing IL-2 production in response to

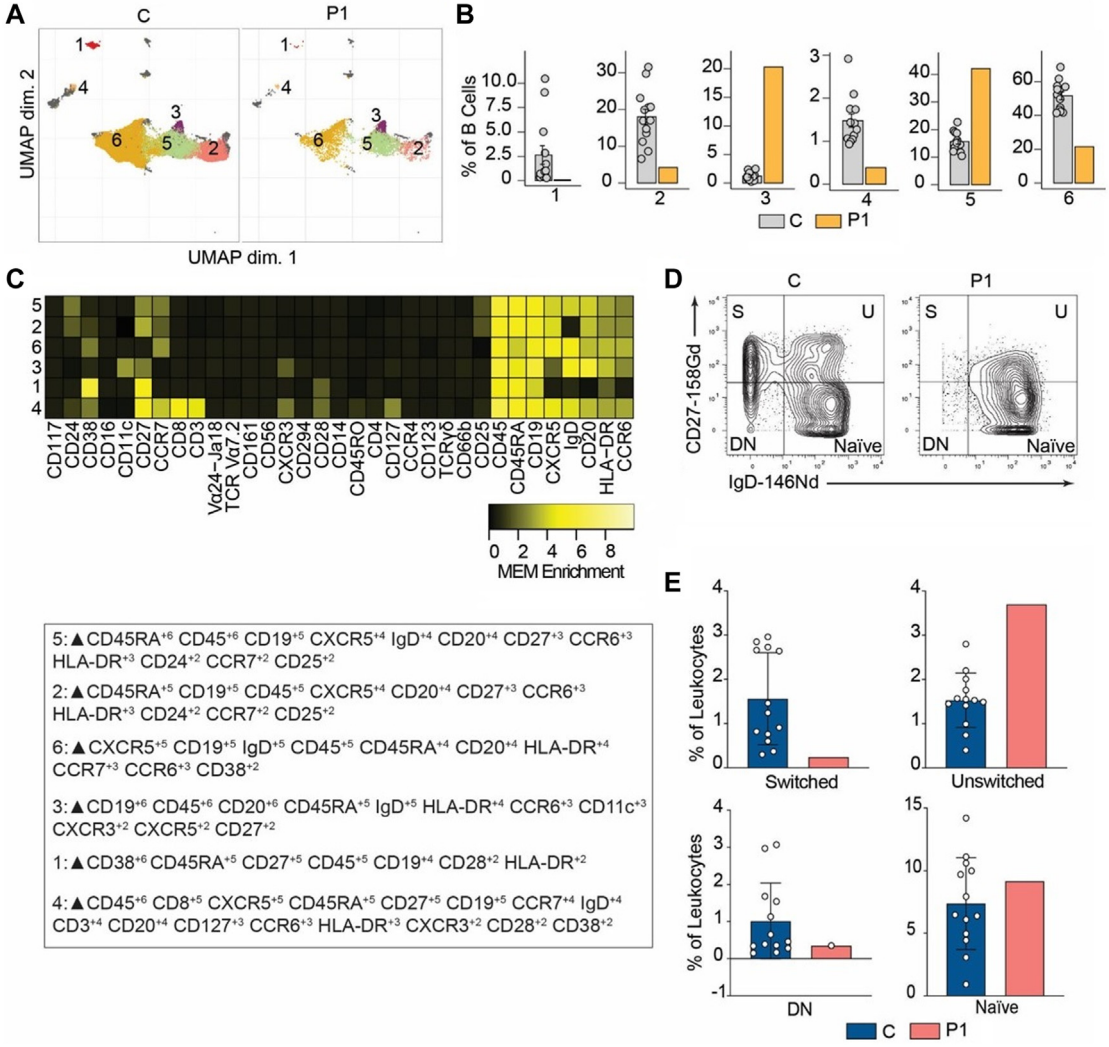


**FIG 4.** B-cell immunophenotyping. **(A)** UMAP representation showing B-cell population from Fig 2. Each *color* represents a cluster obtained by unsupervised clustering with FlowSOM; 10,000 cells from healthy controls (C) and patient (P1) are represented. **(B)** Frequencies of FlowSOM clusters highlighted in *(A)* as percentage of total cells in B-cell population from Fig 2. **(C)** MEM heat map and marker tags for clusters shown in *(A)*. Markers differentially expressed between clusters are indicated in *bold*. **(D)** CD27 versus IgD B cells, with manual gating on samples from C and P1. **(E)** Frequencies of naive, double-negative, switched, and unswitched B cells in C and P1 as percentage of leukocytes obtained by manual gating. *UMAP,* Uniform manifold approximation and projection.

**TABLE II.** Distribution of lymphocyte subpopulations in peripheral blood

| Characteristic | % P1 | % I2 (mother) | % II1 (sibling) | % Internal healthy age-matched control* | % Healthy controls (aged 19-25 years)† |
|---|---|---|---|---|---|
| Lymphocytes | 26.24 | | | 21.39 | 25.5-39.4 |
| $CD19^+$ | 14.87 | 5.30 | 6.79 | 9.70 | 6.6-10.8 |
| Naive $CD27^-IgD^+$ | 75.76 | 66.86 | 82.92 | 75.69 | 65.6-79.6 |
| Nonswitched memory $CD27^+IgD^+$ | 18.42 | | | 10.20 | 7.4-13.9 |
| Switched memory $CD27^+IgD^-$ | 3.05 | 11.29 | 11.29 | 10.95 | 7.2-12.7 |
| Transitional $CD24^{++}CD38^{++}$ | 1.16 | | | | 1.0-3.6 |
| Plasmablast $CD27^{++}CD38^{++}$ | 0 | | | | 0.6-1.6 |
| NK $CD3^-CD56^+$ | 15.20 | 9.97 | 21.61 | 6-29 | |

Distribution of lymphocyte subpopulations in peripheral blood of P1.
*Internal reference values (age range, 25-50 years).
†According to the values of Morbach et al.[29]

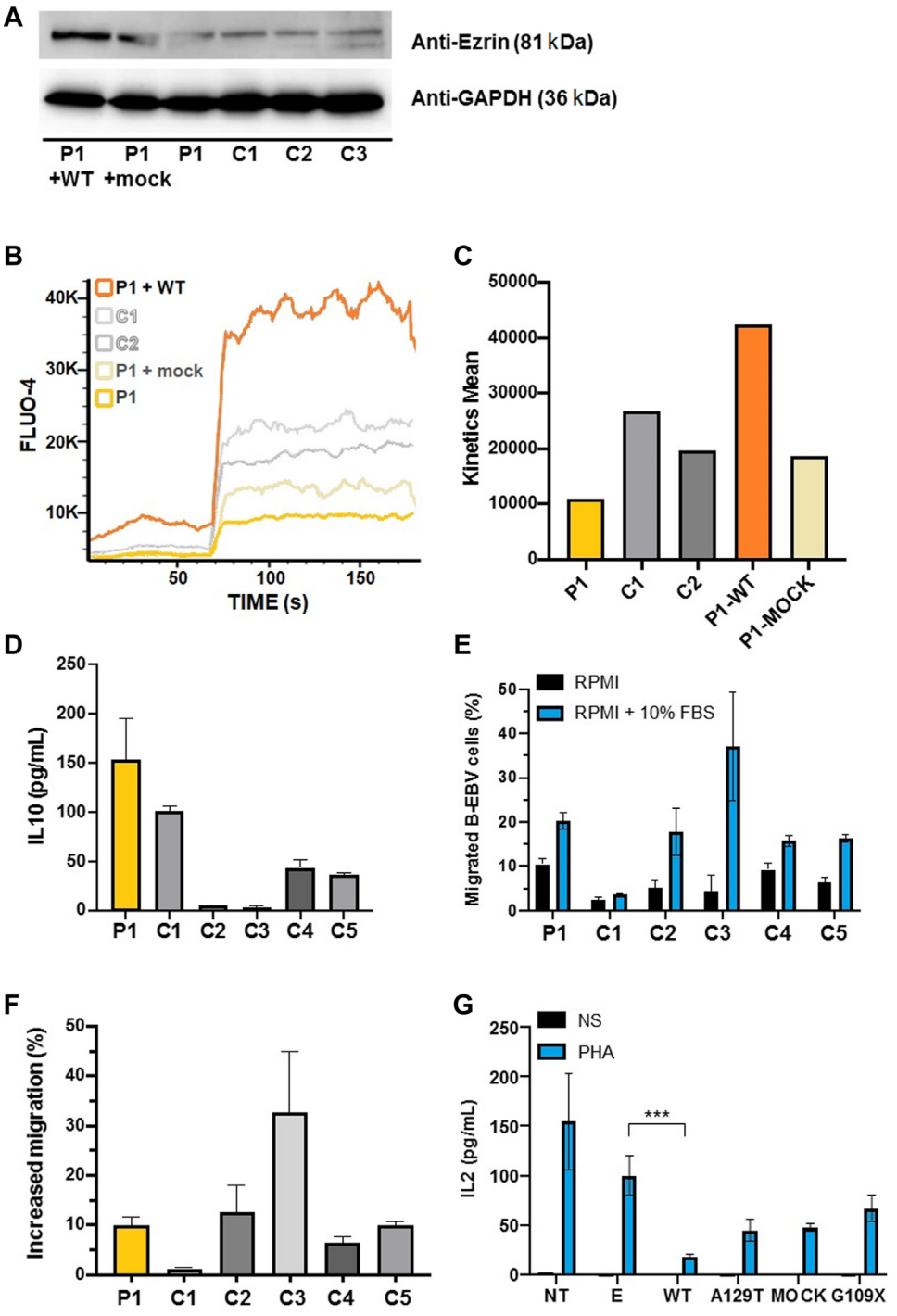


**FIG 5.** Impact of human ezrin deficiency on B-cell and T-cell signaling. **(A)** Immunoblot analysis of ezrin in EBV-B cells from patient (P1) transfected with *EZR*-WT plasmid (P1 + WT), cells from P1 transfected with mock vector (P1 + Mock), untransfected cells from P1, and healthy controls (C1–C3). GAPDH was used as loading control. Control shown is representative of 3 controls analyzed. Results are shown from a single experiment, representative of 3. **(B)** Calcium flux analysis in EBV-B cells in response to ionomycin for P1, P1 + Mock, P1 + WT, C1, and C2. Results are shown from a single experiment, representative of 3. **(C)** Calcium flux (mean change in fluorescence on y-axis) is represented for P1, P1 + Mock, P1 + WT, C1, and C2 in ionomycin-stimulated EBV-B cells. In Kruskal-Wallis (nonparametric) tests comparing differences between healthy control and patient under same conditions, $*P = .0286$ for difference between P1 and C2 and $****P < .0001$ for difference between P1 and C3. Results are shown from a single experiment, representative of 3. **(D)** Production of IL-10, as assessed by ELISA, in EBV-B cells from patient (P1) and 5 healthy controls (C1–C5). Means ± SDs were calculated from 3 independent experiments. Kruskal-Wallis (nonparametric) tests comparing differences between healthy controls and patient under same conditions; $*P = .0286$ for difference between P1 and C2 and $****P < .0001$ for difference between P1 and C3.

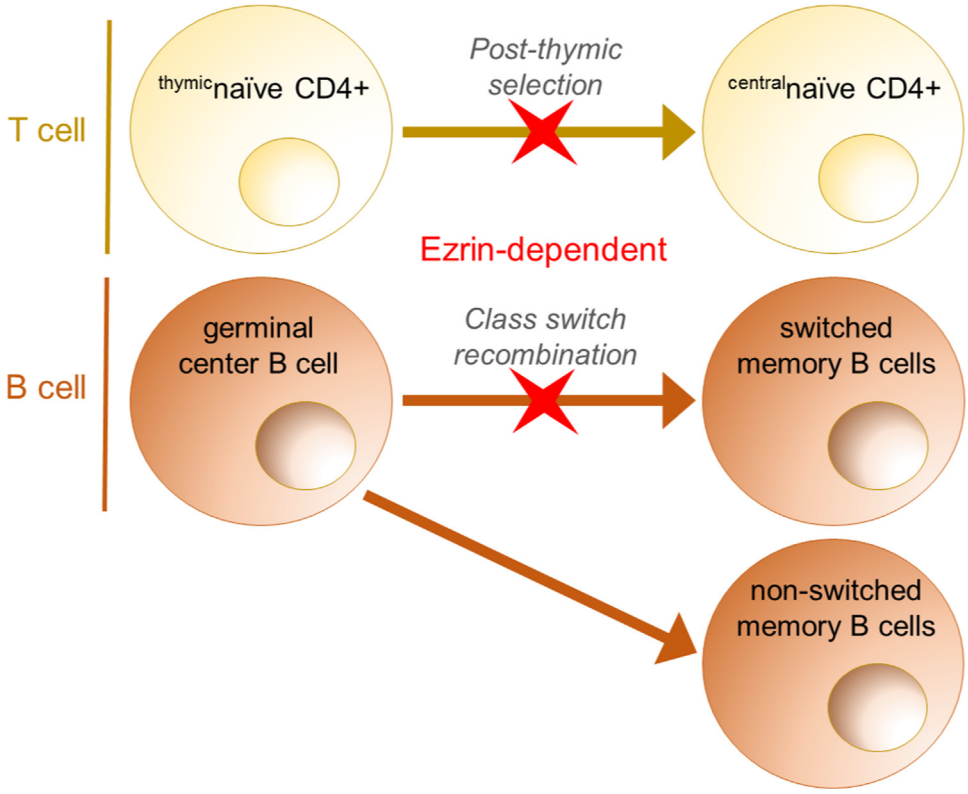


**FIG 6.** Summary of ezrin-dependent and -independent T- and B-cell subpopulations from patient (P1).

PHA stimulation (Fig 5, *G*). As expected, mock transfection and the G109X plasmid had no effect on IL-2 production in response to PHA stimulation (no significant difference relative to cells subjected to electroporation in the absence of plasmid E) (Fig 5, *G*). The overproduction of WT ezrin decreased IL-2 production after PHA stimulation (***$P < .001$ for comparison of plasmid E and WT), whereas the overproduction of A129T had no effect on IL-2 production. This decrease in IL-2 production with WT ezrin was not due to an increase in cell mortality because the same numbers of transfected cells were recovered for all transfections. The overexpression of the A129T and WT forms of ezrin therefore had opposite effects on TCR signaling in Jurkat T cells (Fig 5, *G*). Our data suggest that ezrin regulates IL-2 expression and that this function is abolished by the mutation.

## DISCUSSION

We describe here the first case of B-cell deficiency caused by an autosomal-recessive complete deficiency of ezrin. Unlike ezrin-deficient mice, which appear normal at birth but die within 7 to 10 days,[41] the patient presented with a mild version of B-cell deficiency and survived into adulthood with appropriate care. The lethality in mouse is thought to be due to defects in the apical terminal web of the gut epithelium, a tissue in which ezrin is the only ERM complex protein expressed, excluding the possibility of redundancy with moesin or radixin.[42] However, the normal T-cell development and only partial defects of TCR-induced IL-2 production and $Ca^{2+}$ signaling observed in mice with a conditional knockout of ezrin in T cells[24,26] suggest that ezrin may have different functions in mice and humans, highlighting the importance of studying IEI to elucidate the basic mechanisms of human immunity. Further reinforcing this dichotomy between humans and mice, human ezrin deficiency results in a decrease in the size of several T-cell subpopulations ($CD4^+$, $CD8^+$, MAIT, γδ T, and $^{central}$naive $CD4^+$ T cells; see Table E5 in the Online Repository at www.jacionline.org and Fig 6). Similarly, for the B-cell compartment, the patient presented a decrease in the size of the switched memory B-cell compartment (Fig 6) and an impairment of humoral immunity,

**(E)** Percentage of EBV-B cells migrating in forward FBS gradient for P1 and C1–C5. Means ± SDs were calculated from 3 independent experiments. **(F)** Percentage difference in migration of EBV-B cells between RPMI 1640 medium and RPMI 1640 + 10% FBS medium for P1 and C1–C5. Means ± SDs were calculated from 3 independent experiments. Differences between P1 and C1–C5 were not significant by Kruskal-Wallis tests (nonparametric). **(G)** Production of IL-12, as assessed by ELISA, Jurkat T cells left nonstimulated (NS), or stimulated with PHA (PHA) for Jurkat T cells that were not transfected (NT), were electroporated without plasmid (E), transfected with *EZR*-WT plasmid (WT), transfected with *EZR*-A129T mutant plasmid (A129T), transfected with mock vector (MOCK), or transfected with *EZR*-G109X mutant plasmid (A129T). Means ± SDs were calculated from 3 independent experiments. Kruskal-Wallis (nonparametric) tests were performed to evaluate differences between Jurkat T cells electroporated without plasmid *(E)* and cells transfected with various constructs (WT, A129T, MOCK, and G109X) in the same conditions; ***$P < .001$ for difference between E and WT. *GAPDH*, Glyceraldehyde phosphate dehydrogenase.

whereas conditional ezrin deletion in the B-cell lineage in mice resulted in normal levels of the various B-cell subsets and an increase in antibody production.[25] It is not possible to draw conclusions about the preservation of other phosphorylation-independent functions of ezrin that might account for the milder phenotype of the patient. On the one hand, our data show that the A129T mutation causes B-cell deficiency and suggest that human and murine ezrin proteins have different functions (Table E5), including a normal cell migration in the patient's cells. On the other hand, A129T mutation was studied in comparison with the WT form of ezrin, showing that in spite of there being no change in the plasma membrane localization of the mutant form in NIH3T3 cells, A129T mutation is unable to bind Ras protein and deregulates Ras-dependent cellular processes.[43] Although the studies were performed with the suspicion that it could be related to intellectual disability, this fact was not validated,[43] although the elegant study on A129T mutation complements and reinforces the pathogenicity of the mutation. Moreover, we were unable to obtain fibroblasts from the skin biopsy samples from the patient, even after 2 attempts. Ezrin is strongly expressed in skin, and its role in the biogenesis of epithelial junctions[44] suggests that ezrin deficiency may impair fibroblast development (Fig E6).

The work presented here increases our knowledge of the proteins of the ERM complex and their crucial roles in human immunity. Before this report, the only human gene encoding an ERM complex protein for which mutations had been reported was *MSN*.[5-7] There are some similarities between moesin and ezrin deficiencies in humans. Both deficiencies result in hypogammaglobulinemia and mild lymphopenia (specifically, $CD4^+$, $CD8^+$, MAIT, γδ T, and switched memory B cells), suggesting some redundancy of function between these 2 proteins.[5-7] However, moesin-deficient patients have a more profound T-cell deficiency, accounting for their more severe clinical phenotype, with a higher susceptibility to infection; most $CD8^+$ T cells express the senescence marker CD57, and T-cell proliferation is impaired in these patients.[5-7] The patient with ezrin deficiency had no impairment of T-cell proliferation, but thymic selection was blocked in the periphery, where almost all the $CD4^+CD45RA^+$ cells were $^{thymic}$naive $CD4^+$T cells ($CD4^+CD45RA^+CD31^+$), with no $^{central}$naive $CD4^+$ T cells ($CD4^+CD45RA^+CD31^-$) detected,[45] highlighting the dependence of this stage on ezrin (Fig 6). These findings also suggest that despite belonging to the same family of proteins, ezrin, moesin, and radixin have various redundant and independent roles. Future studies with additional ezrin-deficient patients and new patients with IEI related to radixin should help to shed more light on these issues.

In conclusion, we describe here for the first time an IEI that should be considered in the genetic testing of patients with defects of cellular and humoral immunity for whom no genetic diagnosis has yet been established.

## DISCLOSURE STATEMENT

Supported by Instituto de Salud Carlos III (ISCIII) through the project PI22/00790 and PI17/00543 and co-funded by the European Union, Ayudas Luis Álvarez 2022 FIBHULP, and MINECO RTI2018-095673-B-I00. B.G.S. is supported by PEJD2019-PRE/BMD-16556 Predoctoral Fellowships CAM and ESID Bridge Fellowship. A.V.D.R. received support from Instituto de Salud Carlos III (ISCIII) through the project PI17/00543. J.J.P.C. was funded in part by National Institutes of Health (NIH) training fellowship T32GM139800 and the Initiative for Maximizing Student Development at Vanderbilt. R.M.B. was funded in part by Clinical and Translational Science Award (CTSA) award UL1 TR002243 from the National Center for Advancing Translational Sciences and the National Institute of Allergy and Infectious Diseases of the NIH (grant R21AI171466). The Laboratory of Human Genetics of Infectious Diseases is supported by the Howard Hughes Medical Institute, Rockefeller University, the St Giles Foundation, the NIH CTSA program (UL1TR001866), and the French National Research Agency (ANR) under the "Investments for the Future" program (ANR-10-IAHU-01), the Integrative Biology of Emerging Infectious Diseases Laboratory of Excellence (ANR-10-LABX-62-IBEID), the French Foundation for Medical Research (EQU201903007798), the SCOR Corporate Foundation for Science, the Institut National de la Santé et de la Recherche Médicale (INSERM), REACTing-INSERM, and the University of Paris Cité.

Disclosure of potential conflict of interest: The authors declare that they have no relevant conflicts of interest.

We thank the patient and her family for participating in this study.

**Clinical implications: We describe the first case of autosomal-recessive ezrin deficiency in a patient with hypogammaglobulinemia and low frequencies of switched memory B, $CD4^+$ and $CD8^+$ T, MAIT, γδ T, and $^{central}$naive $CD4^+$ cells.**

## REFERENCES

1. Notarangelo LD, Bacchetta R, Casanova JL, Su HC. Human inborn errors of immunity: an expanding universe. Sci Immunol 2020;5:eabb1662.
2. Fehon RG, McClatchey AI, Bretscher A. Organizing the cell cortex: the role of ERM proteins. Nat Rev Mol Cell Biol 2010;11:276-87.
3. Gupta N, Upadhyay M, Cheung M, Bhunia N. Ezrin. Encyclopedia of signaling molecules. Cham: Springer; 2018:1665-73. https://doi.org/10.1007/978-3-319-67199-4_101745
4. Song W, Liu C, Upadhyaya A. The pivotal position of the actin cytoskeleton in the initiation and regulation of B cell receptor activation. Biochim Biophys Acta Biomembr 2014;1838:569-78.
5. Lagresle-Peyrou C, Luce S, Ouchani F, Soheili TS, Sadek H, Chouteau M, et al. X-linked primary immunodeficiency associated with hemizygous mutations in the moesin (MSN) gene. J Allergy Clin Immunol 2016;138:1681-9.e8.
6. Delmonte OM, Biggs CM, Hayward A, Comeau AM, Kuehn HS, Rosenzweig SD, et al. First case of X-linked moesin deficiency identified after newborn screening for SCID. J Clin Immunol 2017;37:336-8.
7. Bradshaw G, Lualhati RR, Albury CL, Maksemous N, Roos-Araujo D, Smith RA, et al. Exome sequencing diagnoses X-linked moesin-associated immunodeficiency in a primary immunodeficiency case. Front Immunol 2018;9:420.
8. Satooka H, Nagakubo D, Sato T, Hirata T. The ERM protein moesin regulates $CD8^+$ regulatory T cell homeostasis and self-tolerance. J Immunol 2017;199:3418-26.
9. Kikuchi S, Hata M, Fukumoto K, Yamane Y, Matsui T, Tamura A, et al. Radixin deficiency causes conjugated hyperbilirubinemia with loss of Mrp2 from bile canalicular membranes. Nat Genet 2002;31:320-5.
10. He XJ, Wang WR, Zhang Y, Yang Q. The effect of radixin knockdown on the expression and efflux function of MRP2 in SGC-7901 cells. Eur J Pharm Sci 2012;46:426-34.
11. Kitajiri S, Fukumoto K, Hata M, Sasaki H, Katsuno T, Nakagawa T, et al. Radixin deficiency causes deafness associated with progressive degeneration of cochlear stereocilia. J Cell Biol 2004;166:559-70.
12. Li H, Durbin R. Fast and accurate short read alignment with Burrows-Wheeler transform. Bioinformatics 2009;25:1754-60.
13. McKenna A, Hanna M, Banks E, Sivachenko A, Cibulskis K, Kernytsky A, et al. The Genome Analysis Toolkit: a MapReduce framework for analyzing next-generation DNA sequencing data. Genome Res 2010;20:1297-303.

14. Wang K, Li M, Hakonarson H. ANNOVAR: functional annotation of genetic variants from high-throughput sequencing data. Nucleic Acids Res 2010;38:e164.
15. Pellat-Deceunynck C, Jego G, Harousseau JL, Vie H, Bataille R. Isolation of human lymphocyte antigens class I–restricted cytotoxic T lymphocytes against autologous myeloma cells. Clin Cancer Res 1999;5:705-9.
16. Garcia-Solis B, Van Den Rym A, Pérez-Caraballo JJ, Al-Ayoubi A, Alazami AM, Lorenzo L, et al. Clinical and immunological features of human BCL10 deficiency. Front Immunol 2021;12:786572.
17. Nowicka M, Krieg C, Crowell H, Weber L, Hartmann F, Guglietta S, et al. CyTOF workflow: differential discovery in high-throughput high-dimensional cytometry datasets. F1000Research 2019;6:748.
18. Van Gassen S, Callebaut B, Helden M, Lambrecht B, Demeester P, Dhaene T, et al. FlowSOM: using self-organizing maps for visualization and interpretation of cytometry data. Cytometry A 2015;87:636-45.
19. Diggins K, Greenplate A, Leelatian N, Wogsland C, Irish J. Characterizing cell subsets using marker enrichment modeling. Nat Methods 2017;14:275-8.
20. Phang JM, Harrop SJ, Duff AP, Sokolova AV, Crossett B, Walsh JC, et al. Structural characterization suggests models for monomeric and dimeric forms of full-length ezrin. Biochem J 2016;473:2763-82.
21. Itan Y, Zhang SY, Vogt G, Abhyankar A, Herman M, Nitschke P, et al. The human gene connectome as a map of short cuts for morbid allele discovery. Proc Natl Acad Sci U S A 2013;110:5558-63.
22. Oleaga-Quintas C, de Oliveira-Júnior EB, Rosain J, Rapaport F, Deswarte C, Guérin A, et al. Inherited GATA2 deficiency is dominant by haploinsufficiency and displays incomplete clinical penetrance. J Clin Immunol 2021;41:639-57.
23. Michie KA, Bermeister A, Robertson NO, Goodchild SC, Curmi PMG. Two sides of the coin: ezrin/radixin/moesin and merlin control membrane structure and contact inhibition. Int J Mol Sci 2019;20:1996.
24. Shaffer MH, Huang Y, Corbo E, Wu GF, Velez M, Choi JK, et al. Ezrin is highly expressed in early thymocytes, but dispensable for T cell development in mice. PLoS One 2010;5:e12404.
25. Pore D, Parameswaran N, Matsui K, Stone MB, Saotome I, McClatchey AI, et al. Ezrin tunes the magnitude of humoral immunity. J Immunol 2013;191:4048-58.
26. Shaffer MH, Dupree RS, Zhu P, Saotome I, Schmidt RF, McClatchey AI, et al. Ezrin and moesin function together to promote T cell activation. J Immunol 2009;182:1021-32.
27. Amu S, Tarkowski A, Dörner T, Bokarewa M, Brisslert M. The human immunomodulatory $CD25^{+}$ B cell population belongs to the memory B cell pool. Scand J Immunol 2007;66:77-86.
28. Wu YCB, Kipling D, Dunn-Walters D. The relationship between CD27 negative and positive B cell populations in human peripheral blood. Front Immunol 2011;2:81.
29. Morbach H, Eichhorn EM, Liese JG, Girschick HJ. Reference values for B cell subpopulations from infancy to adulthood. Clin Exp Immunol 2010;162:271-9.
30. Sasaki Y, Kurosaki T. Immobile BCRs: the safety on the signal trigger. Immunity 2010;32:143-4.
31. Rozsnyay Z, Sarmay G, Zöller M, Gergely J. Membrane-bound ezrin is involved in B-cell receptor–mediated signaling: potential role of an ITAM-like ezrin motif. Immunol Lett 1996;54:163-9.
32. Pore D, Matsui K, Parameswaran N, Gupta N. Cutting edge: ezrin regulates inflammation by limiting B cell IL-10 production. J Immunol 2016;196:558-62.
33. Parameswaran N, Matsui K, Gupta N. conformational switching in ezrin regulates morphological and cytoskeletal changes required for B cell chemotaxis. J Immunol 2011;186:4088-97.
34. Hao JJ, Wang G, Pisitkun T, Patino-Lopez G, Nagashima K, Knepper MA, et al. Enrichment of distinct microfilament-associated and GTP-binding–proteins in membrane/microvilli fractions from lymphoid cells. J Proteome Res 2008;7:2911-27.
35. King LB, Freedman BD. B-lymphocyte calcium influx. Immunol Rev 2009;231:265-77.
36. Gonzalez-Garza MT, Cruz-Vega DE, Maldonado-Bernal C. IL10 as cancer biomarker. In: Sundaresan S, Gu YH, editors. Translational research in cancer. Rijeka: IntechOpen; 2020.
37. Ou-Yang M, Liu HR, Zhang Y, Zhu X, Yang Q. ERM stable knockdown by siRNA reduced *in vitro* migration and invasion of human SGC-7901 cells. Biochimie 2011;93:954-61.
38. Badolato R. Defects of leukocyte migration in primary immunodeficiencies. Eur J Immunol 2013;43:1436-40.
39. Burns SO, Zarafov A, Thrasher AJ. Primary immunodeficiencies due to abnormalities of the actin cytoskeleton. Curr Opin Hematol 2017;24:16-22.
40. Roumier A, Olivo-Marin JC, Arpin M, Michel F, Martin M, Mangeat P, et al. The membrane–microfilament linker ezrin is involved in the formation of the immunological synapse and in T cell activation. Immunity 2001;15:715-28.
41. Saotome I, Curto M, McClatchey AI. Ezrin is essential for epithelial organization and villus morphogenesis in the developing intestine. Dev Cell 2004;6:855-64.
42. Doi Y, Itoh M, Yonemura S, Ishihara S, Takano H, Noda T, et al. Normal development of mice and unimpaired cell adhesion/cell motility/actin-based cytoskeleton without compensatory up-regulation of ezrin or radixin in moesin gene knockout. J Biol Chem 1999;274:2315-21.
43. Riecken LB, Tawamie H, Dornblut C, Buchert R, Ismayel A, Schulz A, et al. Inhibition of RAS activation due to a homozygous ezrin variant in patients with profound intellectual disability. Hum Mutat 2015;36:270-8.
44. Citi S, Guerrera D, Spadaro D, Shah J. Epithelial junctions and Rho family GTPases: the zonular signalosome. Small GTPases 2014;5:1-15.
45. Kohler S, Thiel A. Life after the thymus: $CD31^{+}$ and $CD31^{-}$ human naive $CD4^{+}$ T-cell subsets. Blood 2009;113:769-74.

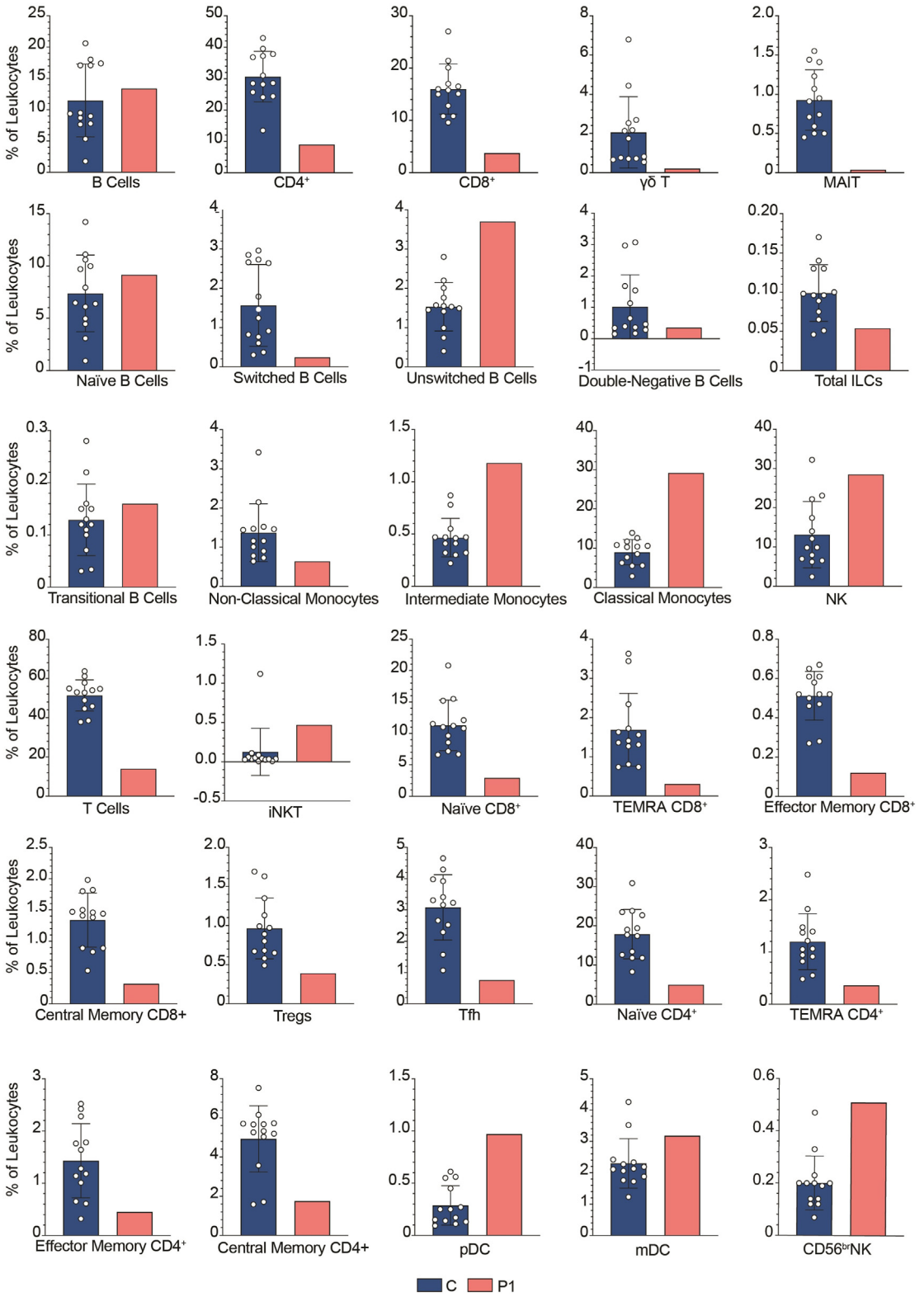


**FIG E1.** Immunophenotyping frequencies determined by manual gating. Frequencies of different populations as percentage of total leukocytes in healthy controls (C) and patient (P1).

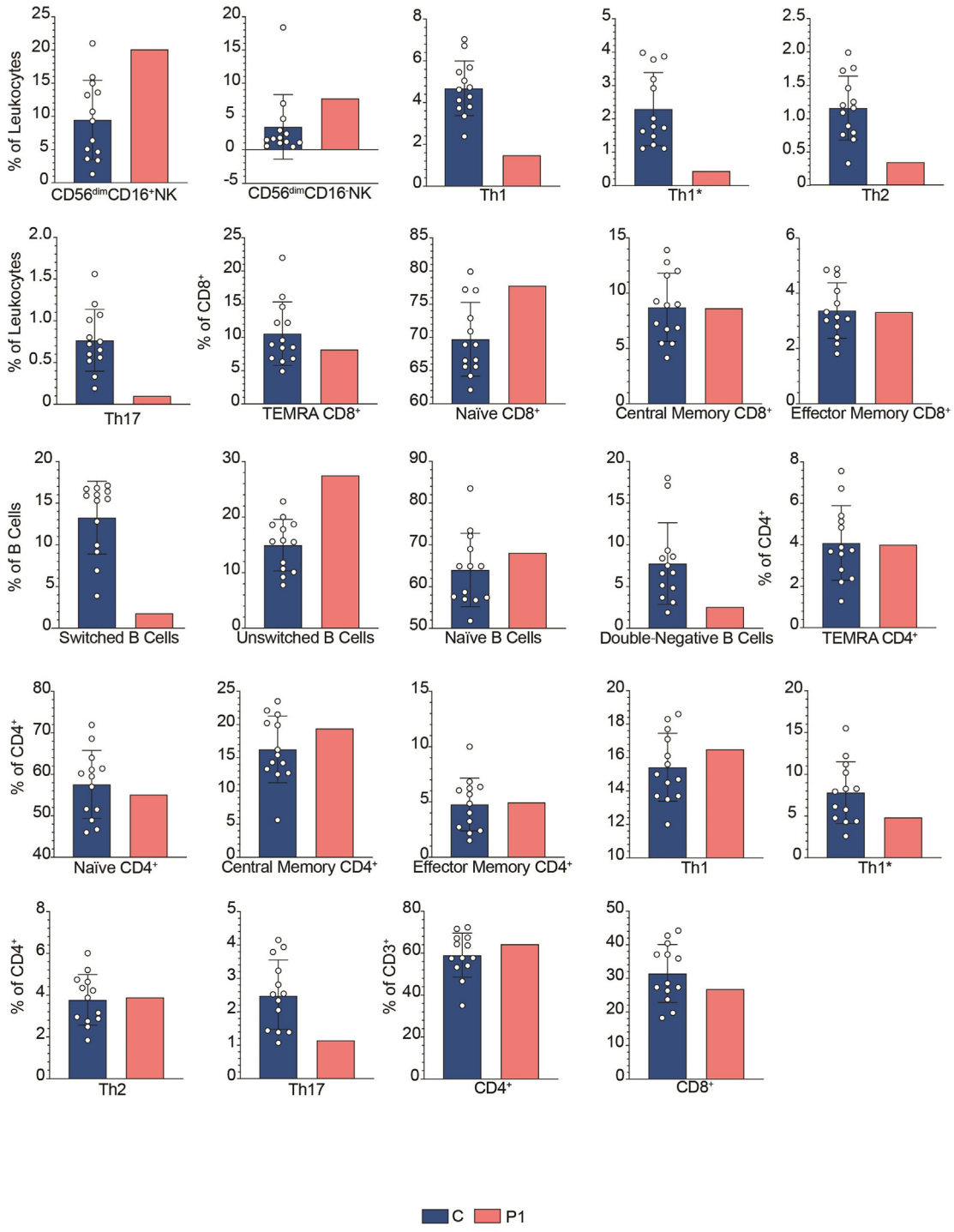


**FIG E2.** Unsupervised analysis of NK and T cells. Frequencies of different populations as percentages of total leukocytes, B cells, or $CD4^+$ cells in healthy controls (C) and patient (P1).

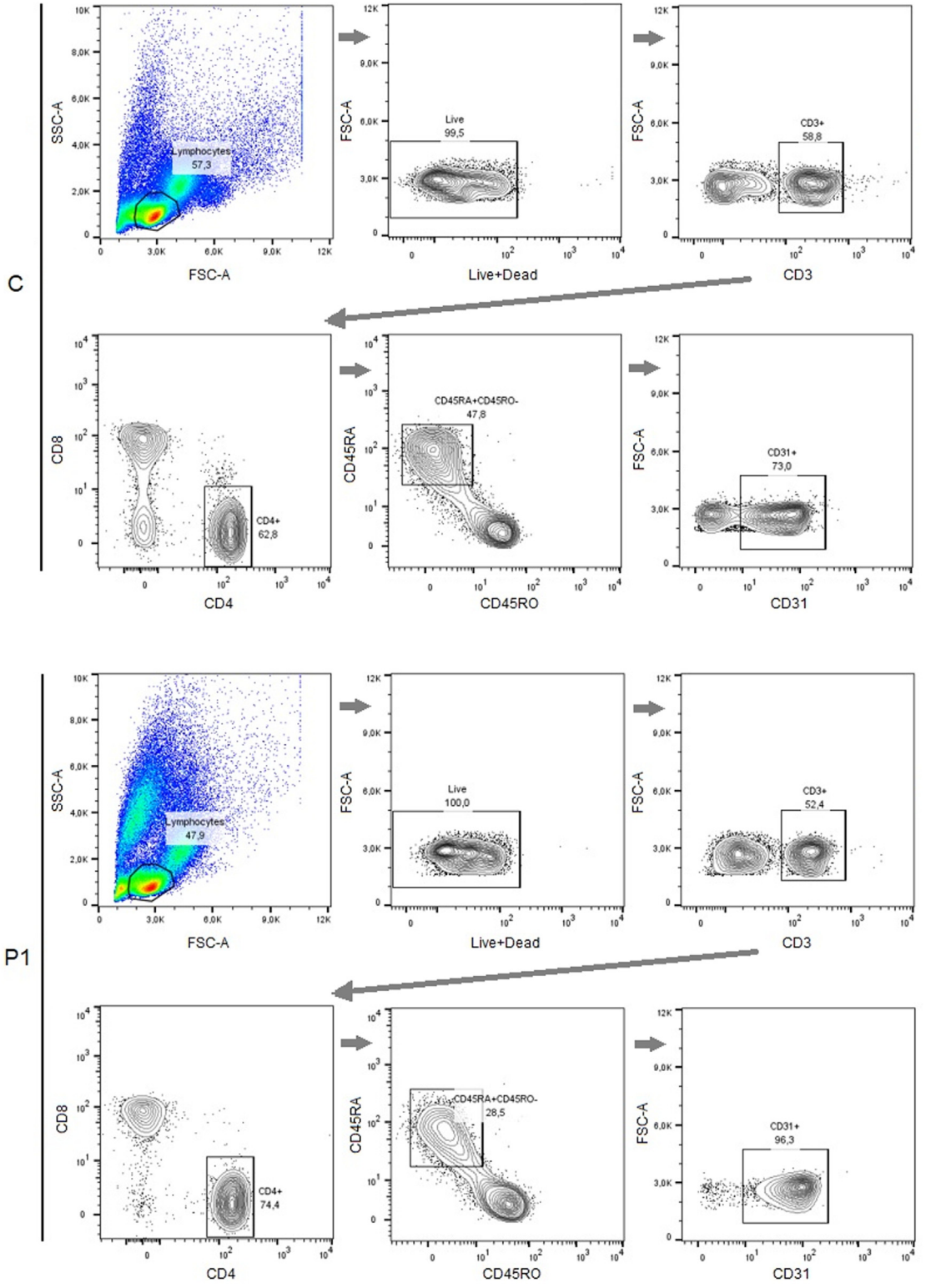


**FIG E3.** Cytometric workflow for $^{thymic}$naive and $^{central}$naive CD4 T-cell analysis. Cytometric workflow for analysis of $^{thymic}$naive CD4 T cells and $^{central}$naive CD4 T cells in healthy control (C) and patient (P1).

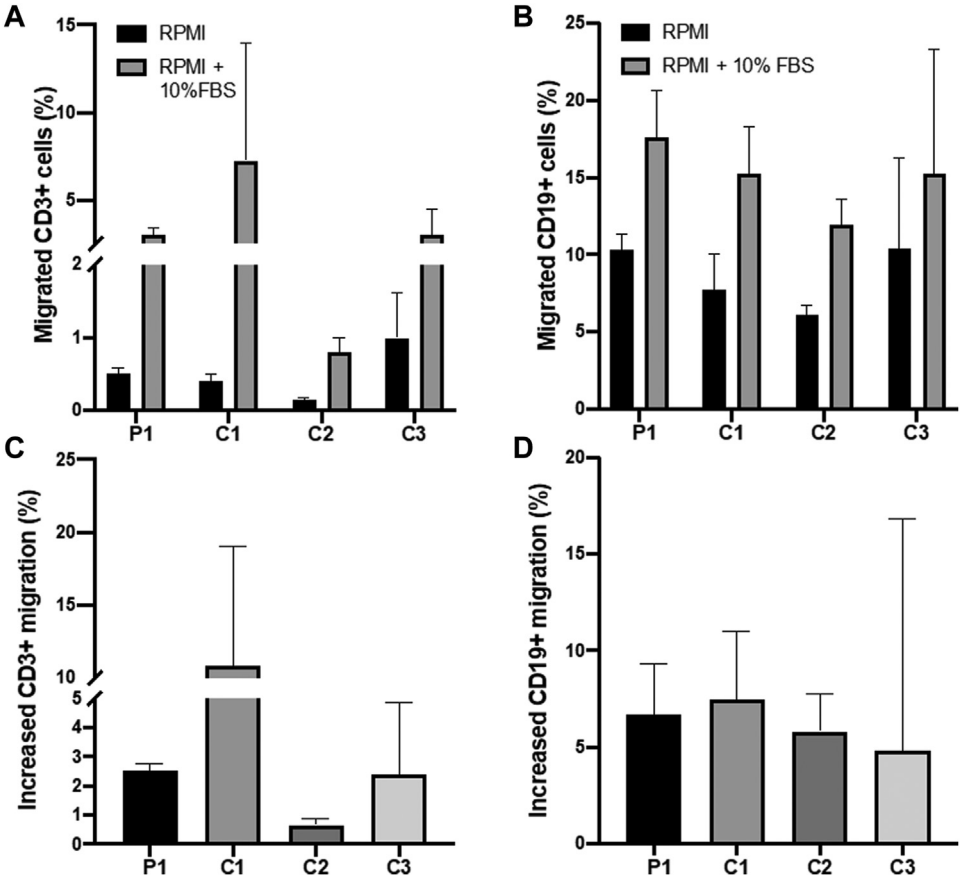


**FIG E4.** Cell migration of B and T cells. Percentage of T cells ($CD3^+$) **(A)** and B cells ($CD19^+$) **(B)** migrating in forward FBS gradient for P1 and C1–C3. Means ± SDs were calculated from 3 independent experiments. Percentage difference in migration of T cells ($CD3^+$) **(C)** and B cells ($CD19^+$) **(D)** between RPMI 1640 medium and RPMI 1640 + 10% FBS medium for P1 and C1–C3. Means ± SDs were calculated from 3 independent experiments. Differences between P1 and C1–C3 were not significant by Kruskal-Wallis tests (nonparametric).

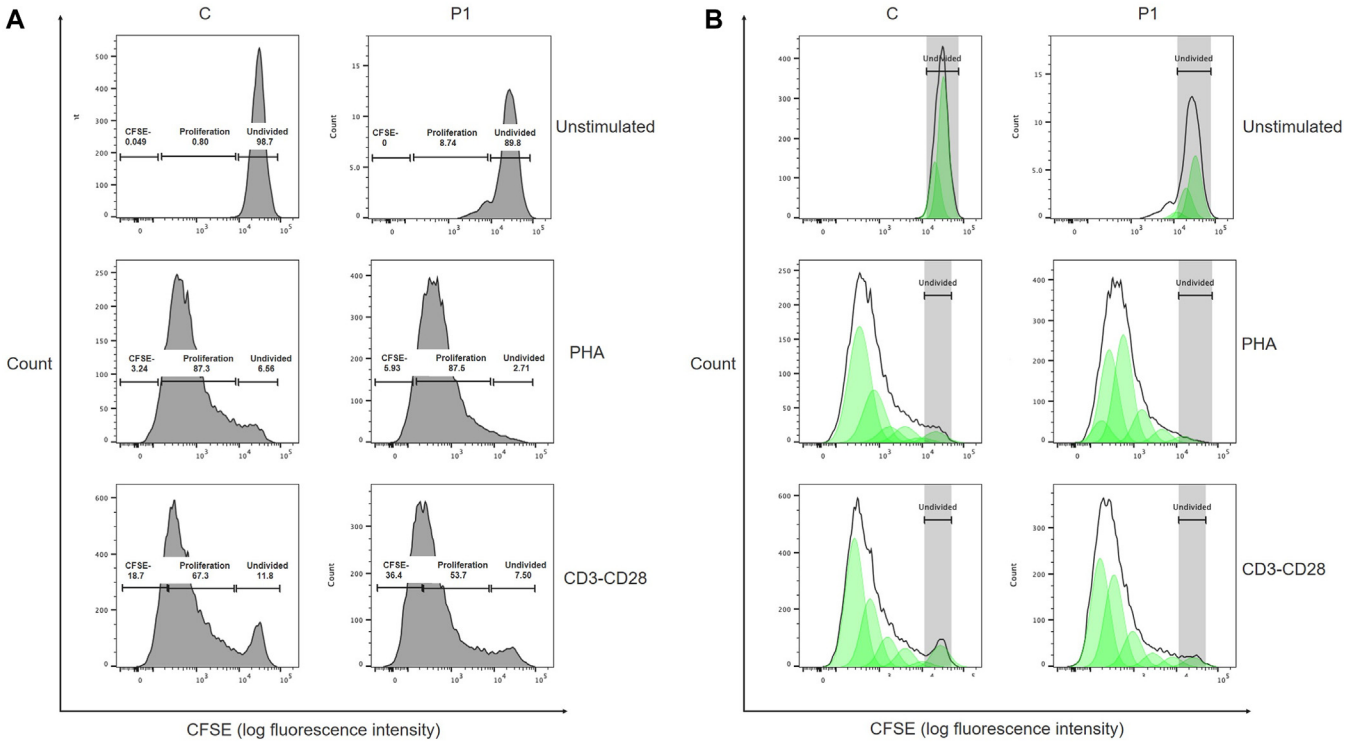


**FIG E5.** Proliferative response of T cells. PBMCs (250,000 cells) were labeled with CFSE and cultured in the presence of PHA or human T-activator CD3/CD28 beads (CD3-CD28) for 6 days. They were then collected, stained, and acquired by a BD FACSCelesta flow cytometer and analyzed by FlowJo. Control (C) is healthy age-matched donor; P1 is patient. **(A)** Histograms showing percentage of cells proliferating or remaining undivided. **(B)** Histograms showing number of cycles of proliferation. Histograms showing populations gated by forward scatter versus side scatter, singlets, and $CD3^{+}$ population. Shown are results representative of 2 independent experiments.

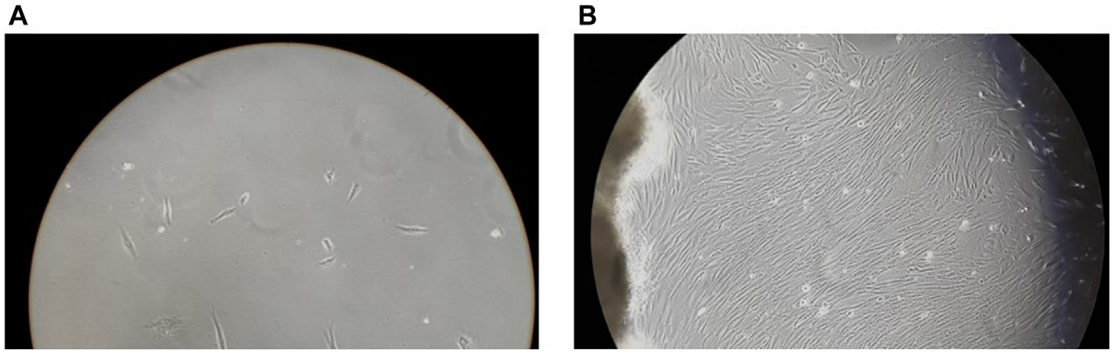


**FIG E6.** Deficient fibroblast growth. Microscopic visualization of human fibroblasts showing much lower levels of fibroblast growth in patient **(A)** than in healthy control **(B)**.

**TABLE E1.** Antibodies used for mass cytometry

| Antibody | Clone | Company | Isotope | Dilution |
|---|---|---|---|---|
| Anti-human CD45 | H130 | Fluidigm | 89Y | 1:50 |
| Anti-human CD19 | HIB19 | Fluidigm | 142Nd | 1:50 |
| Anti-human 127/IL-7Ra | A019D5 | Fluidigm | 143Nd | 1:50 |
| Anti-human CD38 | HIT2 | Fluidigm | 144Nd | 1:50 |
| Anti-human IgD | IA6-2 | Fluidigm | 146Nd | 1:50 |
| Anti-human CD11c | Bu15 | Fluidigm | 147Sm | 1:50 |
| Anti-human CD16 | 3G8 | Fluidigm | 148Nd | 1:50 |
| Anti-human CD194/CCR4 | L291H4 | Fluidigm | 149Sm | 1:50 |
| Anti-human CD123/IL-3R | 6H6 | Fluidigm | 151Eu | 1:50 |
| Anti-human TCR γδ | 11F2 | Fluidigm | 152Sm | 1:50 |
| Anti-human CD185/CXCR5 | RF8B2 | Fluidigm | 153Eu | 1:50 |
| Anti-human CD3 | UCHT1 | Fluidigm | 154Sm | 1:50 |
| Anti-human CD45RA | HI100 | Fluidigm | 155Gd | 1:50 |
| Anti-human CD27 | L128 | Fluidigm | 158Gd | 1:50 |
| Anti-human CD28 | CD28.2 | Fluidigm | 160Gd | 1:50 |
| Anti-human CD66b | 80H3 | Fluidigm | 162Dy | 1:50 |
| Anti-human CD183/CXCR3 | G025H7 | Fluidigm | 163Dy | 1:50 |
| Anti-human CD161 | HP-3G10 | Fluidigm | 164Dy | 1:50 |
| Anti-human CD45RO | UCHL1 | Fluidigm | 165Ho | 1:50 |
| Anti-human CD24 | ML5 | Fluidigm | 166Er | 1:50 |
| Anti-human CD197/CCR7 | G043H7 | Fluidigm | 167Er | 1:50 |
| Anti-human CD8 | SK1 | Fluidigm | 168Er | 1:50 |
| Anti-human CD25 | 2A3 | Fluidigm | 169Tm | 1:50 |
| Anti-human CD20 | 2H7 | Fluidigm | 171Yb | 1:50 |
| Anti-human HLA-DR | L243 | Fluidigm | 173Yb | 1:50 |
| Anti-human CD4 | SK3 | Fluidigm | 174Yb | 1:50 |
| Anti-human CD56 | NCAM16.2 | Fluidigm | 176Yb | 1:50 |
| Anti-human CD196 | G034E3 | Fluidigm | 141Pr | 1:25 |
| Anti-human CD14 | M5E2 | Fluidigm | 175Lu | 1:25 |
| Anti-human CD117 | 104D2 | BioLegend | 150Nd | 1:25 |
| Anti-human TCR Vα24/Jα18 | 6B11 | BioLegend | 156Gb | 1:25 |
| Anti-human TCR Vα7.2 | 3C10 | BioLegend | 159Tb | 1:25 |
| Anti-human CD294 | BM16 | BioLegend | 161Dy | 1:25 |

**TABLE E2.** IgG, IgA, and IgM measured by nephelometry for P1

| | P1 at age: | | | |
|---|---|---|---|---|
| **Immunoglobulin** | **28 years** | **29 years** | **30 years** | **Healthy controls** |
| IgG (mg/100 mL) | 469.00 | 421.00 | 391.00 | 723.00-1685.00 |
| IgA (mg/100 mL) | 20.60 | 16.20 | 21.80 | 69.00-382.00 |
| IgM (mg/100 mL) | 27.90 | 27.40 | 26.80 | 40.00-230.00 |

Internal reference values are age matched.

**TABLE E3.** Immune cell populations in peripheral blood

| Subject | Leukocytes (/mL) | Lymphocytes (/mL) | Platelets (/mL) |
|---|---|---|---|
| Healthy controls | 3,800-10,200 | 1,000-4,800 | 150,000-450,000 |
| P1 at age: | | | |
| 30 years | 3,190 | 1,100 | 129,000 |
| 29 years | 7,750 | 1,330 | 134,000 |
| 27 years | 3,880 | 1,180 | 139,000 |
| 26 years | 4,120 | 1,090 | 121,000 |
| 25 years | 2,71 | 1,06 | 112,000 |

Internal reference values are age matched.

**TABLE E4.** Western blot densitometric analysis

| Subject | EZR (%) | GAPDH (%) | EZR normalized | GAPDH normalized | Ratio (EZR/GAPDH) | % Ratio (EZR/GAPDH) |
|---|---|---|---|---|---|---|
| C1 | 29.88 | 17.01 | 1.00 | 0.65 | 1.53 | 100.00 |
| C2 | 14.08 | 11.88 | 0.47 | 0.46 | 1.03 | 67.47 |
| C3 | 18.22 | 14.20 | 0.61 | 0.54 | 1.12 | 73.06 |
| C4 | 13.18 | 13.55 | 0.44 | 0.52 | 0.85 | 55.37 |
| C5 | 13.46 | 17.27 | 0.45 | 0.66 | 0.68 | 44.36 |
| P1 | 11.18 | 26.09 | 0.37 | 1.00 | 0.37 | 24.40 |

*EZR,* Ezrin; *GAPDH,* glyceraldehyde phosphate dehydrogenase.

**TABLE E5.** Comparison between conditional ezrin knockout in mouse lymphocytes and human ezrin deficiency

| Cell | Conditional ezrin knockout in lymphocytes | Human ezrin deficiency |
|---|---|---|
| T | T-cell development proceeds normally[24,26] | Decrease in size of T-cell subpopulations ($CD4^+$, $CD8^+$, MAIT, γδ T, and $^{central}$naive $CD4^+$ cells) |
| | Partial defects of TCR-induced IL-2 production and $Ca^{2+}$ signaling[24,26] | Normal TCR-induced T-cell proliferation |
| B | Normal B-cell subsets[25] | Low levels of switched memory B cells |
| | High levels of antibody production[25] | Hypogammaglobulinemia |